

**Master Thesis –
Electrical Engineering**

DC Characterization of Silicon Insulation material



DC Characterization of Silicon Insulation material

By

SATISH BUDDHAWAR

in partial fulfilment of the requirements for the degree of

Master of Science
in Electrical Engineering

at the Delft University of Technology,

29th June 2018

Supervisor:	Dr. A. Rodrigo Mor	TU Delft
Thesis committee:	Dr. A. Rodrigo Mor	TU Delft
	Prof. Ir. Peter Vaessen	TU Delft
	Dr. Ir. Milos Cvetkovic	TU Delft
	Ir Aniket Lewarkar	Lovink Eneritech
	Ir. Dennis Bergsma	Lovink Eneritech

This thesis is confidential and cannot be made public until June 28, 2020.

An electronic version of this thesis is available at <http://repository.tudelft.nl/>.

Abstract

The first commercial High Voltage Direct Current (HVDC) transmission link was installed in 1954 between the mainland of Sweden and the island of Gotland. Since then, there is continuous and remarkable development in the HVDC technology making it an efficient way of transmitting bulk power over large distances. Due to the transition towards low carbon electricity, more renewable energy sources are being integrated into the grid. This trend has increased the use of Direct Current (DC) in the electrical networks at low voltage levels.

In the past few decades, space charge phenomenon in HVDC insulation have been investigated. Many techniques have been developed for studying and understanding the space charge phenomenon in the HVDC insulation. Considering the growth of DC in electrical networks, further research into these techniques and development of novel dielectric materials suitable for DC is also progressing at a quick pace.

Earlier studies on space charge phenomenon were performed mainly on Polyethylene, Epoxy, Polymethyl methacrylate and Polycarbonate insulation materials. These studies have indicated that the space charge starts accumulating beyond a threshold value of the electric field and has a strong dependency on temperature as well as the electric field.

Silicon based insulation is also known as silicones. It is a highly stable and fire-resistant fluid. It is used in cable joints, traction transformers and increasingly in compact transformers where higher than normal temperatures are expected. However, it is known that when equipment is used with DC, they are expected to suffer strongly from space charge accumulation. As a result, considerable modifications in the electric field distribution with respect to the Laplacian field occurs, especially in case of voltage polarity inversion. This may cause insulation degradation and premature breakdown.

The conductivity behaviour and the electric field threshold for space charge accumulation are two of the most important parameters for the design of insulation systems under DC conditions. By limiting the electric field in insulation system below the threshold value, space charge accumulation can be minimised.

Reusing the existing AC cable joints under DC conditions could save considerable time as well as money in realising new DC networks. For that, conductivity behaviour and electric field threshold values of the insulation material should be investigated.

The main goal of this thesis is to investigate and characterise silicon insulation material with regards to its conductivity behaviour and the electric field threshold for space charge formation. This study is a first step towards the feasibility of using silicon fluid-based AC cable joints under DC conditions. The silicon insulation samples in liquid as well as cured(solid) state are subjected to conduction current measurements and space charge measurements using pulsed electroacoustic method.

Simulations are performed on a cable joint model in COMSOL Multiphysics. Presence of cured silicon layer results in a divergent current density. This resulted in high field concentration in cured silicon layer.

Contents

1. Introduction	1
1.1 Cable and cable joints	1
1.2 Transition from AC to DC	1
1.3 Need of this study	2
1.4 Space Charges	3
1.5 Approach	3
1.6 Thesis Outline	4
2. Theory of Space Charges	5
2.1 Introduction	5
2.2 Macroscopic view	6
2.2.1 Electrode – dielectric interface	6
2.2.2 Dielectric – dielectric interface	8
2.2.3 In presence of temperature gradient	9
2.2.4 In case of gross inhomogeneities	11
2.2.5 In case of morphological inhomogeneities	11
2.3 Microscopic view	11
2.3.1 Trapping of charge carriers	12
2.3.2 Injection and extraction of charge carriers	13
2.3.3 Conduction mechanism in polymers	15
2.4 Electric field threshold for space charge accumulation	17
2.5 Polymeric structure of silicon insulation	18
2.6 Summary	19
3. Experiments and Simulation	21
3.1 Sample preparation and electrode material	21
3.2 Conduction current Measurements:	23
3.2.1 Test setup	23
3.2.2 Test procedure	24
3.3 Space Charge Measurements	26
3.3.1 Thermal group	26
3.3.2 Acoustic group	27

3.3.3	Optical group	27
3.3.4	General theory behind the Pulsed Electro-acoustic (PEA) method	27
3.3.5	Pulsed Electro-acoustic method for thin plaques	28
3.4	Cable Joint Simulation	34
3.5	Summary	36
4.	Experimental results	37
4.1	Conduction current measurements	37
4.1.1	Cured (solid) silicon insulation	37
4.1.2	Liquid Silicon insulation	43
4.1.3	Discussion on the results of conduction current measurements	49
4.2	Space charge measurements using Pulsed Electro-acoustic method	51
4.3	Cable Joint Simulations	52
	55
5.	Conclusions and Recommendations	59
5.1	Conclusions	59
5.2	Recommendations	60

List of figures

Figure 1.1: Silicon filled (a) Straight through joint (b) Transition joint [1].....	1
Figure 2.1: Electric field and potential distribution, applied voltage $V=10$ kV (a) When no space charges are present (b) in presence of homocharges (c) in presence of heterocharges	7
Figure 2.2: Maxwell capacitor	8
Figure 2.3: Space charge in presence of temperature gradient.....	9
Figure 2.4: Space charges due to fillers in cast resin insulation [12].....	11
Figure 2.5: Crystalline and amorphous structure in polymers [20].....	11
Figure 2.6: Energy band model	12
Figure 2.7: Schematic representation shallow and deep traps in polymers [21].....	13
Figure 2.8: (a) Physical trap, (b) Chemical trap	13
Figure 2.9: Potential barrier at electrode-dielectric interface.....	14
Figure 2.10: Schematic graph showing current density vs voltage for an ideal case of space Charge limited current [20]	17
Figure 2.11: Plot of E vs J (a) and E vs q (b) of a dielectric indicating threshold	18
Figure 2.12: General formula for silicon fluids [22]	18
Figure 3.1: List of experiments	21
Figure 3.2: Air tight test cell for liquid silicon insulation (a) disassembled (b) assembled.....	22
Figure 3.3: Test samples (a) Liquid silicon insulation poured into Teflon mould (b) Cured (solid) silicon insulation sample.....	22
Figure 3.4: Actual test setup for conduction current measurements on solid samples	24
Figure 3.5: Schematic of test setup for conduction current measurements on solid samples ..	24
Figure 3.6: Actual test setup for conduction current measurements on liquid sample	25
Figure 3.7: Time vs Current characteristics of a dielectric after application of DC voltage ...	25
Figure 3.8: Schematic representation of PEA technique for space charge measurement	27
Figure 3.9: Schematic representation of PEA setup used	29
Figure 3.10: Equivalent circuit of the PEA	29
Figure 3.11: Actual PEA setup used (a) Upper part of PEA table (b) Bottom part of PEA table	30
Figure 3.12 Cable joint model used for Simulation	34
Figure 3.13 Boundary conditions used (a) Ground (b) High voltage.....	34
Figure 3.14 Cured silicon layer in cable joint (highlighted in blue)	35
Figure 3.15 Cable joint model with cut lines for electric field comparison.....	35
Figure 4.1 E-J Characteristic of cured Silicon sample at 20°C	37
Figure 4.2 E-J Characteristic of cured Silicon sample at 60°C	38
Figure 4.3 E-J Characteristic of cured Silicon sample at 40°C	38
Figure 4.4 E-J Characteristics of cured Silicon sample at 20°C , 40°C and 60°C	39
Figure 4.5 E- σ Characteristic of cured Silicon sample at 20°C	39
Figure 4.6 E- σ Characteristic of cured Silicon sample at 40°C	40

Figure 4.7 E- σ Characteristic of cured Silicon sample at 60°C.....	40
Figure 4.8 E- σ Characteristics of cured Silicon sample at 20°C, 40°C and 60°C	41
Figure 4.9 Conductivity of cured silicon vs reciprocal of absolute temperature, at an applied electric field of 2.5 kV/mm	42
Figure 4.10 Temperature vs Electric field threshold.....	43
Figure 4.11 Current (i) and conductivity (σ) vs. stress duration in insulating liquids and relationship with today's standard measuring methods for conductivity determination.....	44
Figure 4.12 Time-current characteristics of Liquid Silicon Insulation at 20°C	45
Figure 4.13 Time-current characteristics of Shell S4 mineral oil at 20°C	45
Figure 4.14 Time-current characteristics of liquid Silicon insulation 20°C.....	46
Figure 4.15 Time-current characteristics of liquid Silicon insulation 40°C.....	46
Figure 4.16 E-J characteristics of liquid Silicon insulation at 20°C.....	47
Figure 4.17 E-J characteristics of liquid Silicon insulation at 40°C.....	47
Figure 4.18 E- σ characteristics of liquid Silicon insulation at 20°C	48
Figure 4.19 E- σ characteristics of liquid Silicon insulation at 40°C	48
Figure 4.20 Dismantled test cell after conduction current measurements with traces of cured silicon on (a) Measuring electrode, (b) High voltage electrode	49
Figure 4.21 Electric field distribution in a co-axial cylinder with dielectric material as (a) XLPE and (b) Cured Silicon insulation.....	51
Figure 4.22 Acoustic pressure signal received at the oscilloscope	52
Figure 4.23 Electric field along cut line 2 when temp gradient is 30°C.....	53
Figure 4.24 Electric field along cut line 1 when temp gradient is 30°C.....	53
Figure 4.25 Electric field along cut line 4 when temp gradient is 30°C.....	54
Figure 4.26 Electric field along cut line 3 when temp gradient is 30°C.....	54
Figure 4.27 Electric field along cut line 1 when temp gradient is 60°C.....	55
Figure 4.28 Electric field along cut line 2 when temp gradient is 60°C.....	55
Figure 4.29 Electric field along cut line 4 when temp gradient is 60°C.....	56
Figure 4.30 Electric field along cut line 3 when temp gradient is 60°C.....	56

List of Tables

Table 3.1 Specifications of the PEA setup used.....	29
Table 3.2 Acoustic properties of the different materials in the PEA setup [28,30]	30
Table 3.3 Property of liquid silicon insulation used in simulations	36
Table 3.4 Properties of materials used in simulation	36
Table 4.1 Electric field and temperature dependency coefficients	41
Table 4.2 Standards for measurement of conductivity or resistivity of insulating liquids.....	43

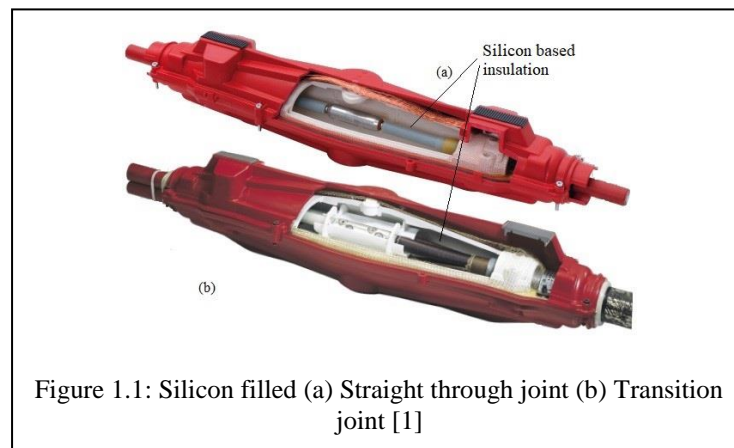
1. Introduction

1.1 Cable and cable joints

Electrical power is transmitted through either overhead lines or underground cables. Each of these transmission types has its benefits as well as drawbacks. However, due to the requirement of high reliability and considering environmental concerns, underground cable systems are taking over from overhead lines. Other benefits of cable systems include: they are out of sight, require less right of way, emit no electric field and have better power loss characteristics.

Cables are manufactured in limited lengths due to the limitation in handling large lengths of cables. To make a longer cable system, specialized connection components are used to put together individual cables. These components are known as cable joints.

There are different types of cable joints such as straight joint, transition joint, etc. However, they share a similar design: a metallic connector to connect the cable cores or conductors; insulation material around the connector; a flexible metallic braid to connect the outer layer of cable on each side. Figure-1.1 below shows the interior view of a silicone filled straight through joint (a) and transition joint (b). The free space around the connector and cable insulation is filled with liquid silicon insulation (fluid silicones).



The behaviour of cable joints is well understood under AC conditions. However, under DC, the electric field distribution differs from that at AC. The field distribution at DC is determined by the conductivity (σ) of the insulation instead of the dielectric permittivity (ϵ_r) for AC. The conductivity depends strongly on the temperature and the electric field. Surface charges and space charges play an important role too. As a result, the electric field distribution is space, time and temperature dependant. This makes the determination of the electric field at DC far more complex than at AC.

1.2 Transition from AC to DC

In the beginning of the electricity era, power was transmitted and distributed at AC. This was mainly because of the two important features of AC i.e. ease of transforming the voltage level and ease of breaking the circuit (current interruption). This AC was perfectly adequate for the

power systems requirements for much of the 20th century. However, considering the growth of renewables, storage systems and DC loads, DC is gradually being more preferred over AC.

This transition from AC to DC is most visible at both high voltage levels as well as low voltage levels. This is mainly because of the technical advancements in the field of power electronics (HVDC and FACTS), power conversion units for end user applications that provide more options for use of DC power at these levels. However, in the medium voltage level, it is mostly limited to isolated systems like rail industries, shipping industries, data centres, telecommunication systems and electrical vehicles. Based on the experience with such existing MVDC systems, research is being carried out on both technical and financial aspects of medium voltage DC grids [2-3]. Studies performed till now on this topic has indicated that offshore DC grids e.g. collector fields for wind farms and small scale industrial networks have been identified as applications in which DC might have an advantage over conventional AC distribution in terms of power quality issues, efficiency, flexibility and cost [4-7].

Under AC, grid infrastructure behaviour is well understood based on the experience of failures and outages of the components. However, the lack of operational know-how of the grid infrastructure under DC could affect the reliability of DC networks [8]. Once this is known, it can be expected to see further increase in the rate of DC use in this transition.

1.3 Need of this study

The cable system consists of cables, cable joints, termination kits, separable connectors, etc. In the transition from AC to DC electrical networks (refurbishing) or hybrid electrical networks, reusing the existing cable system will not only reduce the infrastructural cost but also save the time that would be spent in realising a new infrastructure. Also, there are other technical advantages like high power transfer capability, lower losses, better power quality, avoiding phase imbalances that occurs under AC, etc. [9].

However, except for few laboratory projects, the experiences of an AC cable system running under DC are very limited till today. In such laboratory projects, studies were performed considering only the power system limitations excluding the cable and cable joint reliability factor [8,10]. In a similar way, studies on advantages and challenges in using existing MVAC distribution cables under DC conditions have been performed in [9] along with a novel idea of dynamic rating to overcome the challenge.

The reliability of cables and cable joints can be established from the dielectric properties of insulation materials. These properties include the electrical conductivity and its dependence on temperature and electric field, electric field threshold and space charge development, DC breakdown performance and sensitivity to electrical aging [11]. Each of these properties are insulation material dependant and are not predictable yet.

In this thesis, study has been performed on silicon-based insulation material to check if it can accumulate space charges when operated under DC. This material, in liquid state is currently being used as medium voltage AC cable joint insulation. It has a property to get cured (solidify) when exposed to moisture. This study focusses on understanding and determining the electrical conductivity and its dependence on the electric field and temperature of the

material in liquid as well as solid state under DC conditions. The results of this study also provide an estimate for the threshold value for space charge formation under DC.

1.4 Space Charges

One of the intrinsic characteristics of the insulation under DC voltage is the accumulation of space charges [12]. Insulating materials allow weak electrical conduction. This weak flow of electrical charges is often not uniform because of local-inhomogeneity of the material or presence of temperature gradient, etc. Space charge accumulates when there is an imbalance in the rate at which charge enters and leaves a region.

Under AC voltage, charge has very little chance to penetrate deeply into the insulation material and stay there as the voltage changes its polarity 100 times (for 50Hz supply) per second. Voltage of same polarity under DC environment injects charges that can travel deep into the insulation. Because of the conductivity difference between the conductor and insulation, often the insulation is not capable of transporting all injected charges. This creates an unbalance between charges injected and charges transported in the bulk of insulation resulting in the charge accumulation in the insulation over time [12]. The space charges accumulate in the dielectric at a rate that is dependant primarily on the voltage level, temperature, properties of the insulation and of the electrodes.

The space charges in the dielectric will modify the Laplacian field distribution in the equipment, resulting in an increased magnitude of field in one region than other. This also makes the calculation of electric field in DC complex. Furthermore, increased electric stress levels leads to the increased rates of electrical aging and accelerated failure.

The accumulated charges in the insulation can be released by short circuiting and grounding the electrodes on both sides of the insulation. The rate of such discharging can be increased by increasing the temperature.

Conventional models for the calculation of electric field consider free moving, equally distributed charges alone and the effect of field and temperature on them. The space charge phenomenon in insulation is highly material dependant and not predictable yet.

1.5 Approach

Conduction current measurements at electric fields in the range of 1 kV/mm to 10 kV/mm and temperature in the steps of 20°C, 40°C and 60°C have been performed on solid silicon insulation material to obtain the conductivity dependence on the electric field and temperature. Similar experiments on liquid silicon insulation material have been performed for electric fields between 0.1 kV/mm-5 kV/mm and at temperatures of 20°C and 40°C.

The plot of current density (J) vs applied electric field (E) on a log-log scale from conduction current measurements gives information about the threshold value of electric field for space charge formation in the material.

The conductivity behaviour obtained from conduction current measurements is used to calculate the electric field distribution in a real cable joint model.

Pulsed electro-acoustic method, a non-destructive method is used to verify the electric field threshold values obtained from the conduction current measurements.

1.6 Thesis Outline

The aim of this study is to electrically characterise the silicon insulation material with regards to its conductivity behaviour and threshold for space charge formation under DC voltage. It can further be detailed as:

- a. Do Silicon based insulation accumulate space charges?
- b. To determine the DC conductivity and its dependence on the electric field and temperature
- c. Determining the electric field threshold values for space charge accumulation
- d. Simulating a real cable joint model under DC with the conductivity behaviour determined using conduction current measurements

The result of this research is one basic step towards understanding the silicon insulation behaviour under DC. The conductivity behaviour information will be useful for simulation purpose. Additional research is required to draw conclusion from the behaviour of a complete cable joint under DC.

Chapter 2 explains the basic background theory behind space charge phenomena. In chapter 3, the principle behind the experimental methods are explained. It is followed by the description of actual test setup used for the experiments.

In chapter 4, the experimental results of the conduction current measurements and space charge measurements are presented and discussed. The space charge measurements using pulsed electroacoustic method were performed to verify the electric field threshold values. A real cable joint model has been constructed for simulations using COMSOL Multiphysics software to get the electric field distribution.

Chapter 5 presents the conclusions drawn from this research study with future recommendations.

2. Theory of Space Charges

In this chapter, background theory of formation of space charges is explained. The parameters related to space charge formation can be measured by conduction current and space charge measurements. In section 2.1, basic information about space charge accumulation and its effects is given. Section 2.2 and section 2.3 explains the space charge formation through macroscopic and microscopic point of view. The concept of electric field threshold for space charge accumulation is discussed in section 2.4. Finally, polymeric structure of the silicon-based insulation materials is given in section 2.5.

2.1 Introduction

Electric field distribution is one of the most important factor for lifetime design of high voltage equipment. It can be determined by using Maxwell's equations provided the charge distribution in the dielectric and its permittivity are known. The corresponding Maxwell's equations are given by:

$$\vec{\nabla} \cdot \vec{D} = \rho = \vec{\nabla} \cdot \epsilon \vec{E} \quad (2.1)$$

$$\vec{\nabla} \cdot \vec{E} = \frac{\rho}{\epsilon} \quad (2.2)$$

Ideally, when voltage (AC or DC) is applied, the resulting charge distribution in the equipment can be predicted from its geometry and permittivity/conductivities of the materials. However, in case of DC application, along with this predicted charge distribution, an additional component is also of importance. It is the accumulation of net charges or space charges in the insulation. This accumulation is hardly predictable and can lead to a significant distortion of the Laplacian electric field. The presence of space charges results in energy storage in the insulation given by equation (2.3). This energy can lead to the separation of charged particles of different polarity in the dielectric. This can lead to an accelerated aging or premature breakdown of the insulation.

$$W_e = \frac{\epsilon_0 \epsilon_r E^2}{2} \quad (2.3)$$

Investigation on space charge in polymers by several authors has indicated that space charge accumulation is closely connected with conduction, charge trapping/detrapping and charge transport mechanisms in these materials [14]. Space charge can arise due to free charges or trapped charges, the processes can be explained as below:

1. Dielectric polarisation: The external electric field orients the charge dipoles in the bulk of dielectric material. The associated space charge can be viewed as a sharp step function at the electrodes.
2. Ion migration: Ionic migration results in the presence of electric field during which, positive charges move towards the negative electrode and vice versa. Difference in the mobility of various charge carriers or the existence of traps results in random volume of charge accumulation near to the electrodes. This type of space charge is known as "heterocharges". Impurities such as by-products from production process are believed to be the cause of such heterocharges.

3. **Charge Injection:** Charges injected at the electrodes generate the space charges near to the interface of electrode-dielectric because of the low conductivity of dielectric. These charges have the same polarity as the electrode and are called “homocharges”. Presence of the conductivity gradient across a dielectric also results in the formation of homocharges.

These processes are strongly dependant on the parameters like temperature, the polarising field and its duration, chemical composition of polymer and material of the electrode, etc. The processes are explained from microscopic as well as macroscopic point of view in sections 2.2 and 2.3 respectively.

Till today, much of the research on space charge accumulation has been performed on polyethylene-based insulation materials [15-17]. Fewer examples of other materials on which research has been performed are: Epoxy, Impregnated paper, Polymethyl methacrylate (PMMA), Polycarbonate- with and without titanium dioxide (TiO₂) filler [18], etc. These works have shown that significant amount of space charge starts building up when the applied electric field is above a threshold value, the so-called threshold for space charge accumulation and has a strong dependency on the temperature and electric field. For the polyethylene-based insulation material, this was verified in [19] by performing conduction current measurements and space charge measurements using the PEA method.

2.2 Macroscopic view

From a macroscopic point of view, space charge accumulates when the current density J is divergent across the insulation i.e. when the flow of charges entering an insulation volume differs from charges exiting the insulation volume. Different regions where such divergence of current density is observed are listed below [12]:

- Electrode – dielectric interface
- Dielectric – dielectric interface
- In the presence of temperature gradient
- In case of gross inhomogeneities
- In case of morphological inhomogeneities

2.2.1 Electrode – dielectric interface

The flow of charged particles through the electrode-dielectric interface depends on charge injection/extraction mechanisms at the interface. And the flow of these charges through the dielectric is determined by the charge transport mechanism in the dielectric. All these mechanisms are electric field and temperature dependant. Any imbalance between these charge injection/extraction and charge transport mechanisms results in the accumulation of space charges. In terms of the current density this can be given by:

$$J_{inj}(E, T) - J_{tra}(E, T) = \Delta J_{interface} \quad (2.4)$$

Where, J_{inj} is the injection current density and J_{tra} is the transported current density. Different scenarios can be given by:

1. $J_{inj}(E, T) = J_{tra}(E, T)$

In this case, the interface is known as ohmic. All the charges injected/extracted at the interface are transported by the dielectric. No space charge formation occurs.

$$2. J_{inj}(E,T) < J_{tra}(E,T)$$

The interface in this case is known as non-ohmic. The interface in this case convey the charges at a slower rate that the dielectric can transport them. It results in the formation of heterocharges near the interface. The heterocharges decreases the electric field and transport current in bulk of the dielectric while increasing the electric field near the interface and injection current. Eventually, a steady state situation is achieved when the two currents coincide.

$$3. J_{inj}(E,T) > J_{tra}(E,T)$$

In this case, the flow of charges from the interface exceeds the rate at which the dielectric can transport them resulting in the formation of homocharges. Homocharges decreases the electric field near the interface and hence the injection current and increases the field in bulk of the dielectric and transport current. Eventually, a steady state situation is achieved when the two currents coincide.

Figure-2.1 below shows the electric field and potential distribution with an applied voltage of 10 kV when there are no space charges and in presence of homocharges and heterocharges in a dielectric.

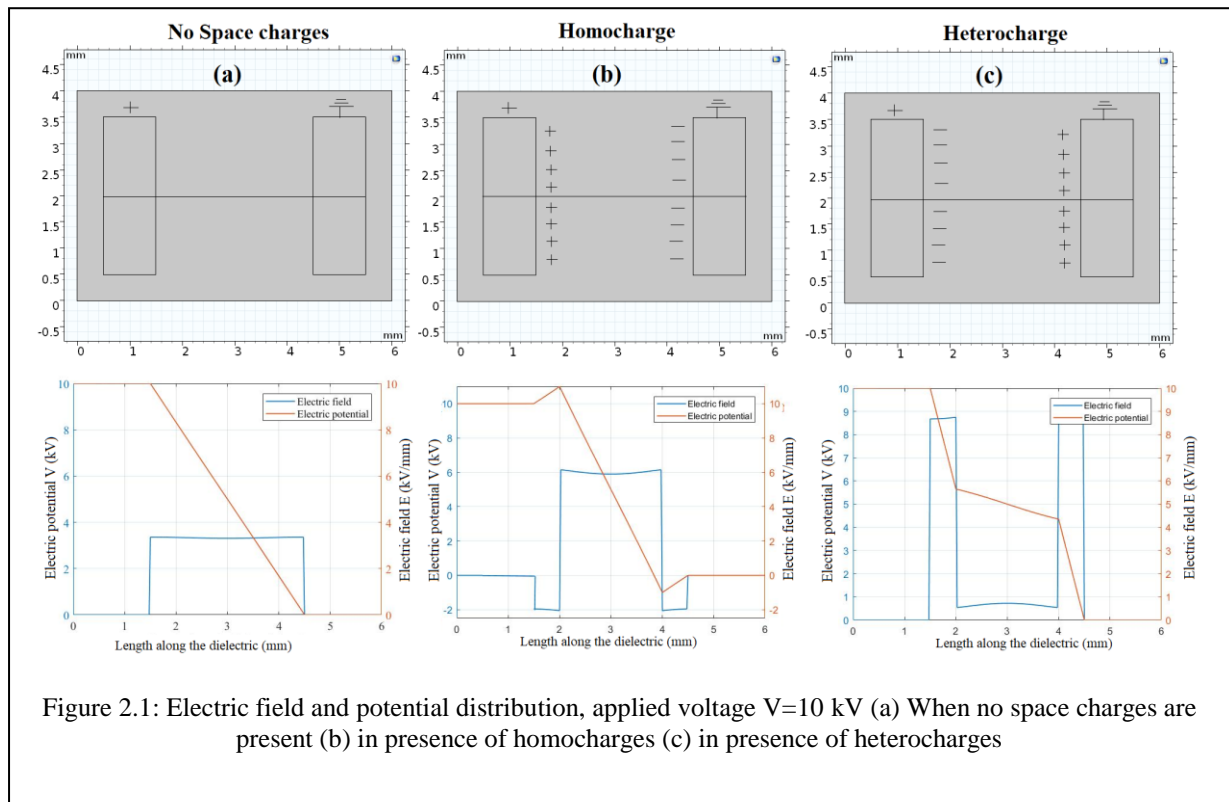
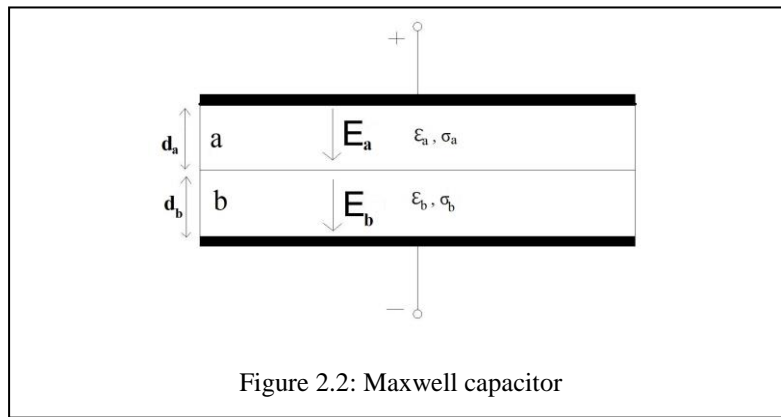


Figure 2.1: Electric field and potential distribution, applied voltage V=10 kV (a) When no space charges are present (b) in presence of homocharges (c) in presence of heterocharges

2.2.2 Dielectric – dielectric interface

The phenomenon at this interface can be explained by the Maxwell-Wagner theory. According to Maxwell-Wagner theory of polarisation, an interfacial charge is formed when the ratio of macroscopic properties permittivity to conductivity of the materials under consideration does not match i.e., $\nabla \left(\frac{\epsilon}{\sigma} \right) \neq 0$.

A hypothetical capacitive configuration as shown in figure-2.2 below is used to describe the phenomenon. It consists of two dielectrics of different permittivity's and conductivities ϵ_a, ϵ_b , and σ_a, σ_b respectively. The thickness of the dielectrics is d_a and d_b respectively.



At time $t=0$, DC voltage U_0 is applied and no space charges are present. The Maxwell's current continuity equations in this case can be given by:

$$J = \sigma E + \frac{d}{dt} D \quad (2.5)$$

$$\nabla \cdot J = 0 \quad (2.6)$$

Combining above equations,

$$\nabla \cdot \sigma E + \frac{d}{dt} \nabla \cdot \epsilon E = 0 \quad (2.7)$$

For the Maxwell capacitor, this results in equation 2.8

$$\sigma_a E_a - \sigma_b E_b + \frac{d}{dt} (\epsilon_a E_a - \epsilon_b E_b) = 0 \quad (2.8)$$

The voltage distribution is given by equation 2.9

$$d_a E_a + d_b E_b = U_0 \quad (2.9)$$

Substituting equation 2.9 into equation 2.8, the value of E_a can be given as

$$E_a = \frac{\sigma_b U_0}{d_b \sigma_a + d_a \sigma_b} \left(1 - \exp\left(\frac{-t}{\tau}\right)\right) + \frac{\varepsilon_b U_0}{d_b \varepsilon_a + d_a \varepsilon_b} \left(1 - \exp\left(\frac{-t}{\tau}\right)\right) \quad (2.10)$$

Where, τ is the time constant and can be given by:

$$\tau = \frac{d_b \varepsilon_a + d_a \varepsilon_b}{d_b \sigma_a + d_a \sigma_b} \quad (2.11)$$

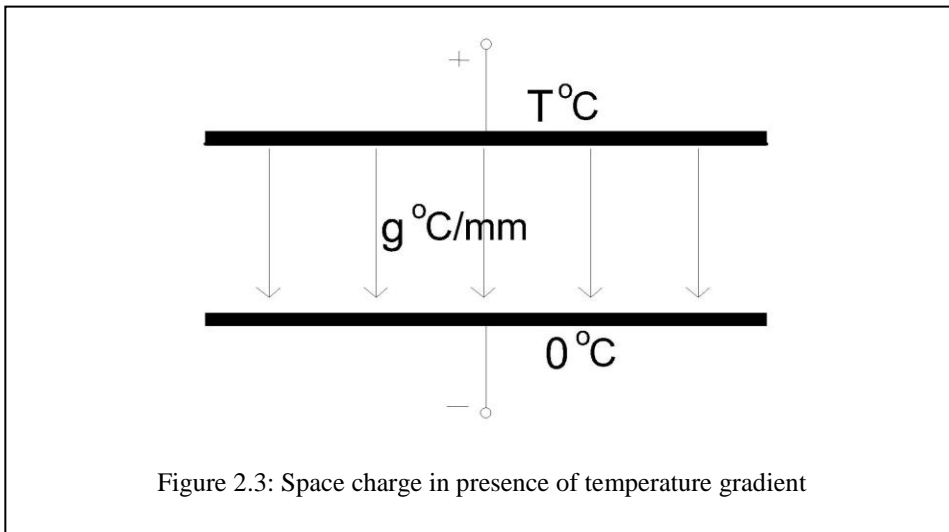
The growth of the surface charge at the interface can be given by:

$$k = \frac{\sigma_b \varepsilon_a - \sigma_a \varepsilon_b}{d_b \sigma_a + d_a \sigma_b} \cdot U_0 \cdot (1 - \exp^{-\frac{t}{\tau}}) \quad (2.12)$$

This indicates that the difference in permittivity's and conductivities of two dielectrics in contact results in divergent current density and electric field distribution. As a result of this, space charge is formed at the interface.

2.2.3 In presence of temperature gradient

Consider a parallel plate configuration with a temperature gradient as top electrode at temperature T with respect to bottom electrode as shown in figure-2.3 below. This causes a temperature gradient $g^\circ \text{C}$ per mm of the dielectric.



The temperature dependency of the conductivity is considered as:

$$\sigma = \sigma_0 e^{\alpha T} \quad (2.13)$$

Where, σ – conductivity of dielectric at temperature T

σ_0 – conductivity of dielectric at 0°C

α – Temperature dependency coefficient of conductivity

The relation between space charge density ρ and the macroscopic properties can be derived from the following Maxwell and current continuity equations:

$$\nabla \cdot \varepsilon E = \rho \quad (2.14)$$

$$J = \sigma E \quad (2.15)$$

Where, ρ – Space charge
 J – Current density
From the above equations,

$$\nabla \cdot \left(\frac{\varepsilon}{\sigma} \cdot J \right) = \rho \quad (2.16)$$

$$J \nabla \cdot \frac{\varepsilon}{\sigma} + \frac{\varepsilon}{\sigma} \nabla \cdot J = \rho \quad (2.17)$$

From the current continuity equation,

$$\nabla \cdot J + \frac{d\rho}{dt} = 0 \quad (2.18)$$

And in static condition, $\frac{d\rho}{dt} = 0$ so that, $\nabla \cdot J = 0$

Therefore,

$$J \nabla \cdot \frac{\varepsilon}{\sigma} = \rho = \sigma E \frac{\sigma \nabla \varepsilon - \varepsilon \nabla \sigma}{\sigma^2} \quad (2.19)$$

Since the permittivity is weakly dependant on temperature, considering $\Delta \varepsilon = 0$, we get,

$$\rho = -\varepsilon E \frac{\nabla \sigma}{\sigma} \quad (2.20)$$

For the considered configuration which is one dimensional case,

$$\rho = -\varepsilon E \frac{1}{\sigma} \frac{d\sigma}{dx} \quad (2.21)$$

Where,

$$\frac{dT}{dx} \text{ can be written as } \frac{dT}{dx} = \frac{d\sigma}{dT} \frac{dT}{dx}$$

and $\frac{dT}{dx}$ is the temperature gradient g .

$$\rho = -\varepsilon E g \frac{1}{\sigma} \frac{d\sigma}{dT} \quad (2.22)$$

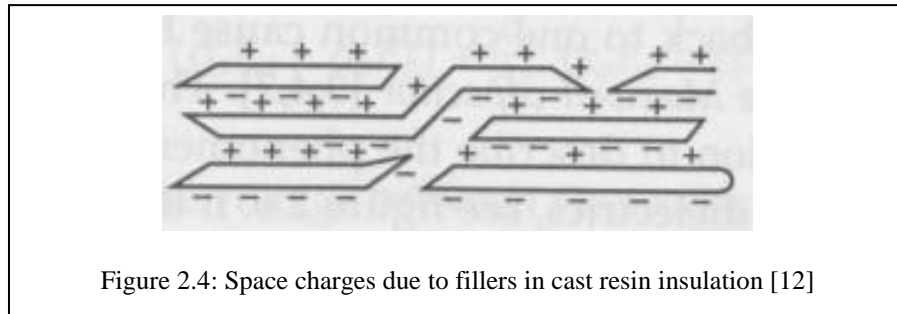
From $\sigma = \sigma_0 e^{\alpha T}$, $\frac{d\sigma}{dT} = \alpha \cdot \sigma_0 e^{\alpha T}$ and $\frac{1}{\sigma} \frac{d\sigma}{dT} = \alpha$

Which gives, $\rho = -\varepsilon \cdot g \cdot \alpha \cdot E$

In a thermally loaded cable or cable joints, a similar scenario exists. The space charge ρ is distributed over the dielectric in proportion to the electric field E and the temperature gradient.

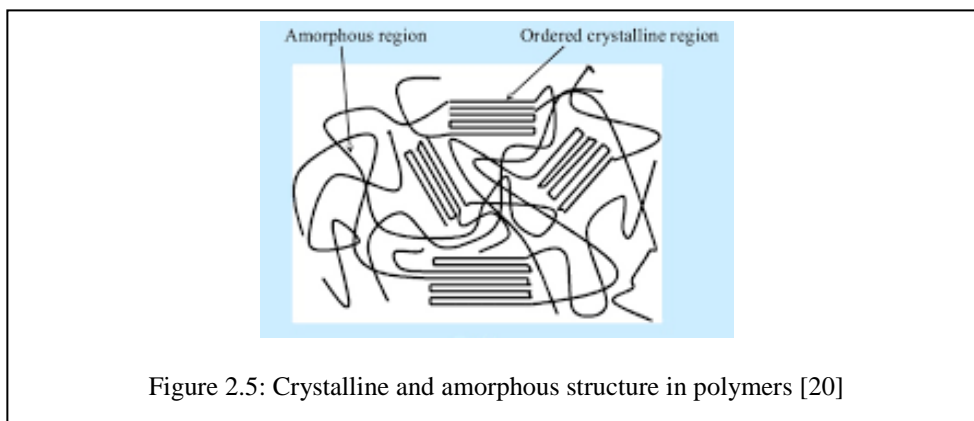
2.2.4 In case of gross inhomogeneities

Quite often fillers are added to the insulating materials to improve the thermal and other properties of materials. The presence of such fillers in the material creates interfaces where $\nabla \left(\frac{\epsilon}{\sigma} \right) \neq 0$. As a result, space charge starts accumulating at these interfaces.



2.2.5 In case of morphological inhomogeneities

In polymers, crystalline and amorphous regions, different conduction properties are observed. The crystalline regions are pure insulators and do not contribute for the conduction. Conduction, if any, takes place in the amorphous regions [12]. Charges start accumulating at the boundary between such crystalline and amorphous regions.



2.3 Microscopic view

From a microscopic point of view, the important mechanisms that are related to the space charge accumulation are [12]:

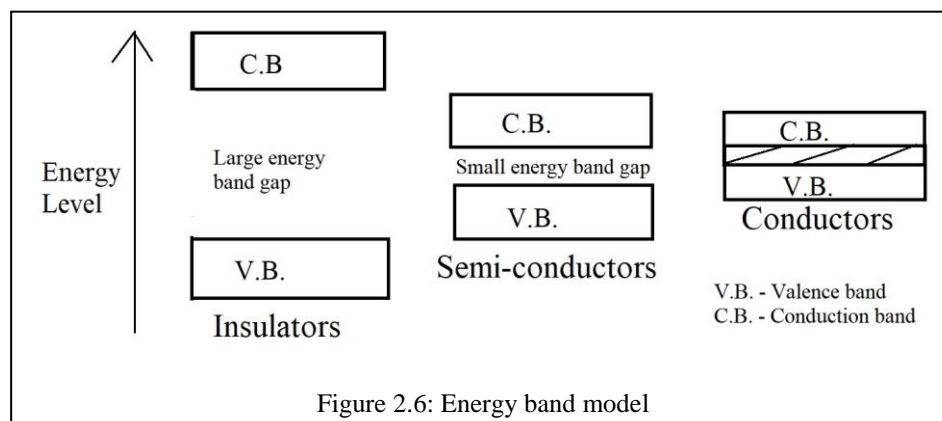
- Trapping of charge carriers
- Injection and extraction of charge carriers
- Conduction of charge carriers

Trapping refers to the fastening of charges at a fixed location in the dielectric. Injection or extraction process occurs at the electrodes and conduction is the transportation of charges through the bulk of the dielectric.

To understand the mechanisms from microscopic point of view, it is essential to differentiate insulators, semi-conductors and conductors based on energy band model. According to Niels Bohr atomic model, a number of electrons move in separate orbits and around the nucleus of an atom. A limited number of orbits which are situated at discrete distances from the nucleus are available. Every orbit represents a distinct energy level. An electron may leap from one orbit to another.

There are two important energy bands, the valence band and the conduction band as shown in figure-2.6. Electrons in the conduction band can easily leap from one atom to another whereas, valence band electrons are firmly connected to the atoms. These two bands are separated by a band gap. This is the forbidden area for the electrons. An electron from the valence band can reach the conduction band only if it attains sufficient energy to pass the forbidden area.

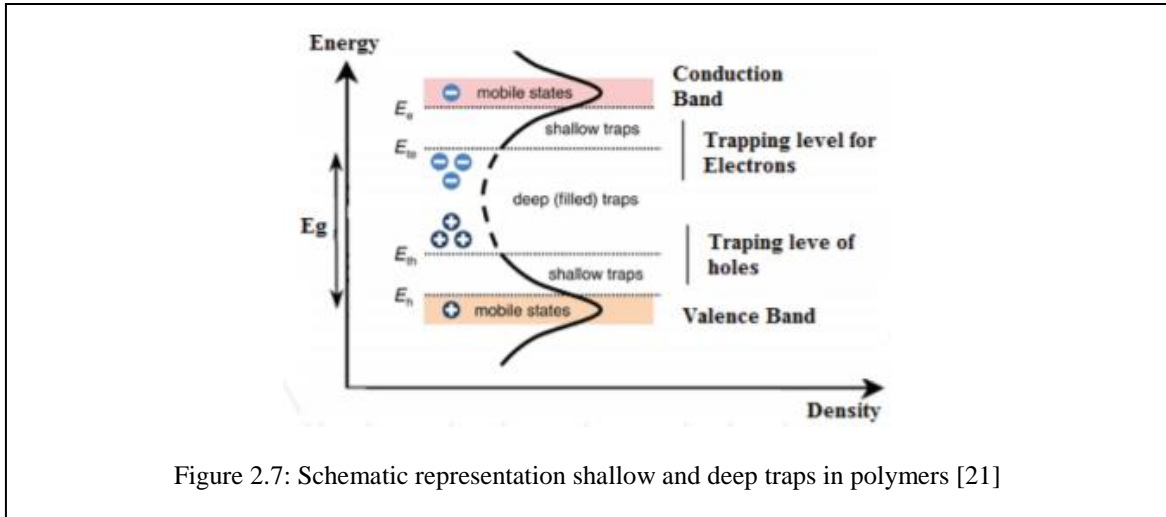
The conductivity of a material depends on the size of this band gap. For insulators, the band gap is larger than 2 eV. For semiconductors it lies in between 0.2 eV and 1 eV and for conductors, the conduction and valence band overlaps, resulting in the band gap less than 0.2 eV.



2.3.1 Trapping of charge carriers

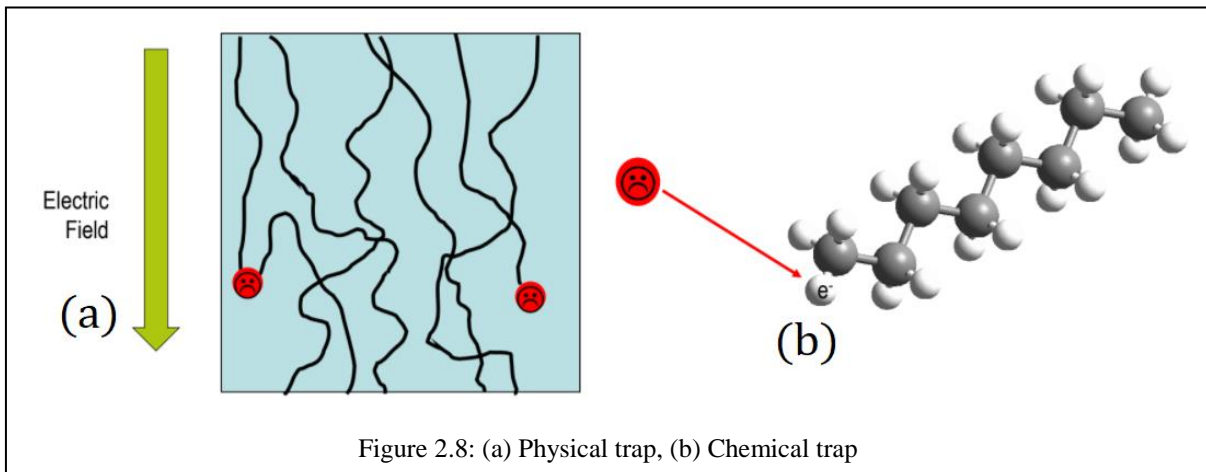
The energy band structure explained in section 2.3 above was originally developed to explain the observed electron energies in the crystalline materials, which was subsequently used in semiconductor theory. However, it can be used to understand the processes in the polymeric materials [20].

Ideally, an insulating material should have valence band and conduction bands. In case of insulating polymers, the physical, conformational or topological disorders results in the localised states at the edge of valence and conduction band that are accessible for charge carriers as shown in figure-2.7. This is because of the existence of traps at these locations.



The traps can be divided into two categories: physical and chemical. In physical traps, charges get “lost” in the impurity locations, material dislocations or defect states in the insulators. In chemical traps, molecular or ionic structures are changed. The chemical traps are generally considered as deeper traps. The charges that trapped in the deep traps require more energy to leave the trap and thus stay in the trap for a longer time than the shallow traps. Self-trap is an example of a chemical trap. It is formed at the location where the field of charges re-orient the local structure of insulation thereby creating a potential well, from which escape may be difficult [12].

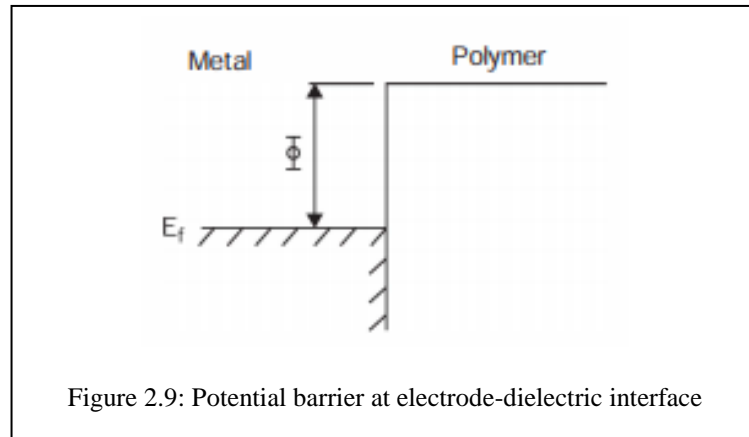
The chemical traps are the results of additives in the polymers. These additives tend to concentrate in the amorphous regions. The type and concentration of the additives have large effects on the number of traps in a polymer.



2.3.2 Injection and extraction of charge carriers

Conduction is possible only if the charge carriers are injected into the polymer. The injection of charge carriers at one electrode interface and extraction at other electrode interface with polymer are the main mechanisms of emission of charges in polymers. Different polymers emit and conducts different charge carriers i.e. either electrons or holes [12].

A potential barrier is believed to exist at the interface of electrode-dielectric as shown in figure-2.9. Charge carriers must gain an amount of energy higher than this barrier height (Φ) to be injected to the polymer. This barrier height can be reduced by electric field.



The two important mechanisms of charge injection are: Schottky injection and Fowler-Nordheim injection.

a. Schottky injection:

When an electric field is applied, the potential barrier height across the electrode – dielectric interface is reduced, making it easy for the charge carriers to cross the barrier. This is mainly because of the thermal emission. The reduction in barrier height (ΔV_m) can be given as

$$\Delta V_m = -e \sqrt{\frac{eE}{4\pi\epsilon_0\epsilon_r}} \quad (2.23)$$

Where, e is the electronic charge, E is the applied electric field, ϵ_0 and ϵ_r are the dielectric permittivity's of air and dielectric respectively. This process is valid for “low” fields of up to 100 kV/mm. The Schottky injection current because of the barrier height reduction can be given by [21]:

$$J = AT^2 \exp \left[-\frac{\left\{ \varphi - e \sqrt{\frac{eE}{4\pi\epsilon_0\epsilon_r}} \right\}}{kT} \right] \text{ A/m}^2 \quad (2.24)$$

Where, A – Richardson’s constant, T is the absolute temperature (in Kelvin) and φ is the barrier height and k is Boltzmann constant.

b. Fowler-Nordheim injection:

This mechanism occurs at very high field, usually above 100 kV/mm. At such high fields, the barrier height becomes very narrow. Despite having insufficient energy, the charge carriers can pass through the barrier by a process of tunnelling. This is also known as high field injection. The injection current density according to this mechanism can be given by:

$$J = BE^2 \exp\left[-\frac{C\varphi^{\frac{3}{2}}}{E}\right] \text{ A/m}^2 \quad (2.25)$$

Where, B and C are empirical constants, E is the applied electric field and φ is the work function of the metal.

This process is called cold tunnelling. It has very small dependence on temperature.

2.3.3 Conduction mechanism in polymers

Conduction in general refers to the flow of charge particles in response to an electric field. In polymeric materials, the charge carriers spend most of their time in the traps and effectively do not contribute to the conduction. The charges that are trapped in deep traps cannot move even if an electric field is applied. Different conduction mechanisms that are believed to take place in the polymers are [20,21]:

- Charge carrier's movement from trap to trap: also known as Poole-Frenkel mechanism
- Tunnelling from one trap site to another: known as resonance tunnelling or thermally assisted tunnelling
- Ionic conduction
- Space charge limited conduction (SCLC)

a. Poole-Frenkel mechanism:

According to this mechanism, high electric fields lower the potential barriers of the traps that localize the charge carriers within the dielectric. This helps in the conduction mechanism where in the charge carriers move from one trap location to another. It is like the Schottky effect where electric field lowers the potential barrier between electrode and dielectric. The current density (J) because of this mechanism is given by:

$$J = \sigma_0 E \exp\left[-\frac{e\varphi - \beta\sqrt{E}}{2kT}\right] \text{ A/m}^2 \quad (2.26)$$

Where, E is the applied electric field, σ_0 is the low field conductivity, β is the Poole - Frenkel constant, k is the Boltzmann constant and T is the absolute temperature.

b. Tunnelling

A charge carrier in a deep trap cannot leave the trap because of its lower energy level to overcome the barrier surrounding it. From quantum mechanics point of view, there is a possibility that the charge carrier can move from one trap site to another via a tunnelling process. The tunnelling process is only allowed to a state with an equal energy. A tunnelling process that takes place at absolute zero temperature is resonance tunnelling.

If the trapped charge carrier is thermally activated by lattice vibrations, it gains energy. Tunnelling to an adjacent trap site is possible, if a charge carrier gains sufficient energy to reach an energetic state equal to an adjacent trap site. This mechanism, which is thermally assisted is termed as thermally assisted tunnelling or hopping mechanism.

c. Ionic Conduction

Current flow cannot occur only because of the electron or hole movement. It also occurs because of the ions. The stable molecular structure in the polymer dissociates into ions that travel through the material in presence of an electric field. It is observed that, the impurities that are the by-products of the production process of the polymer cause ionic conduction. This movement of ions is nothing but the movement of its charged mass which stops at the electrodes since electrodes do not allow mass transport. This results in the formation of heterocharges near the electrodes.

d. Space charge limited conduction (SCLC)

When the injection of charge carriers at electrodes occurs at a rate that is higher than the transport rate of charge carriers in the dielectric, space charge limited conduction occurs.

In case of a trap free dielectric, the charge density is made of two parts, n_0 – intrinsic carrier density and n_1 – injected carrier density from electrodes. The current density (J) in this case can be thought of comprising two components.

$$J = n_0 e \mu \frac{V}{d} (\text{ohmic}) + \frac{9}{8} \frac{\epsilon_0 \epsilon_r \mu V^2}{d^3} (\text{SCLC}) \quad (2.27)$$

Where, V is the applied voltage, d is the distance between electrodes, μ is the mobility of charge carriers and e is the electronic charge.

When $n_1 \ll n_0$, ohmic conduction contribution is overwhelming. And when $n_1 \gg n_0$, the SCLC contribution is overwhelming. By plotting the experimental values of J vs E on a log-log scale system, a transition value of field known as threshold value can be evaluated.

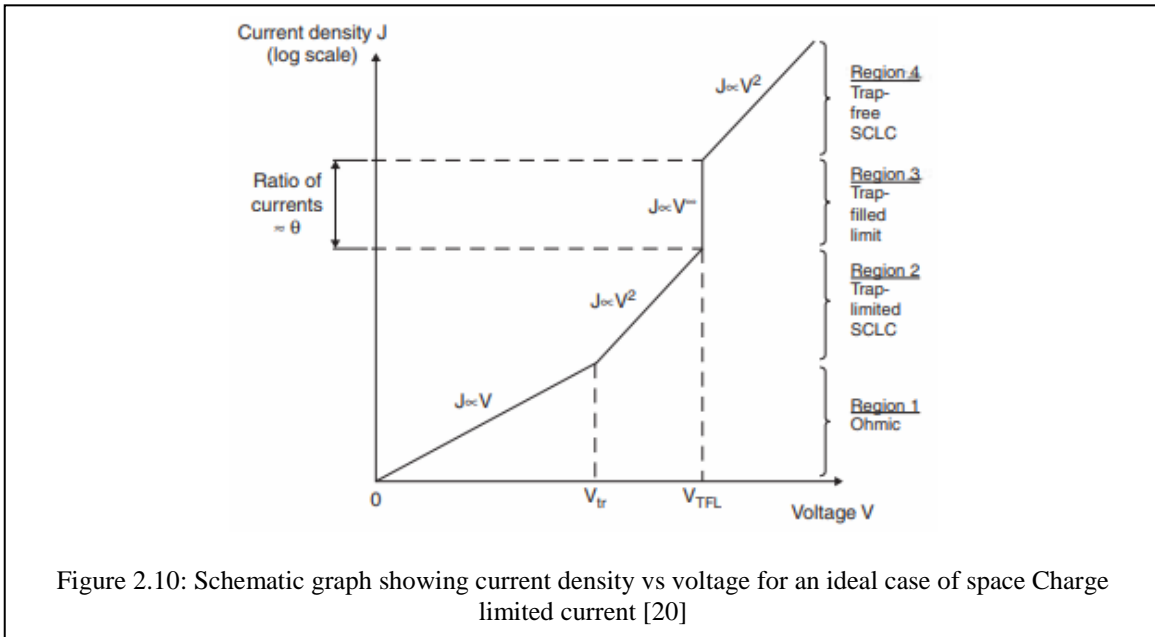
In case of the presence of traps, few of the charge carriers may get trapped into them and do not contribute to the conduction. As a result, only a proportion of charges contribute to the conduction. The current density in this case can be approximated by:

$$J = \theta \frac{9}{8} \frac{\epsilon_0 \epsilon_r \mu V^2}{d^3} \quad (2.28)$$

Where, $\theta = \frac{n_c}{n_t}$, n_c – number of charge carriers available for conduction and n_t – is the number of charge carriers that are trapped.

At higher electric fields, the number of charge carriers injected approximately equals the number of traps. In this case, the traps must be considered deep instead of shallow. When all the traps are filled, the so-called trap-filled limit is reached and the number of electrons available for conduction increases which results in the rapid raise of current density. The value of this current density can be given by:

$$J = \frac{9}{8} \frac{\epsilon_0 \epsilon_r \mu V^2}{S^3} \quad (2.29)$$



These different transitions are schematically shown in figure-2.10 below:

Usually, a power law dependency of the current density J on the electric field is assumed, given by:

$$J = a E^k \quad (2.30)$$

In the low field region, where the ohmic conduction occurs in polymers, the value of k is assumed as 1 in eq. 2.30. This ohmic conduction is because of the travelling of charge carriers along the polymer chains. Charges are trapped and released along these chains. These charges include the free charged particles as well as ions.

Above threshold electric field, also known as super-ohmic region, usually $k=2$ is assumed. The value of k in this case can vary significantly based on the availability of traps and other mechanisms as explained in 2.3.3.

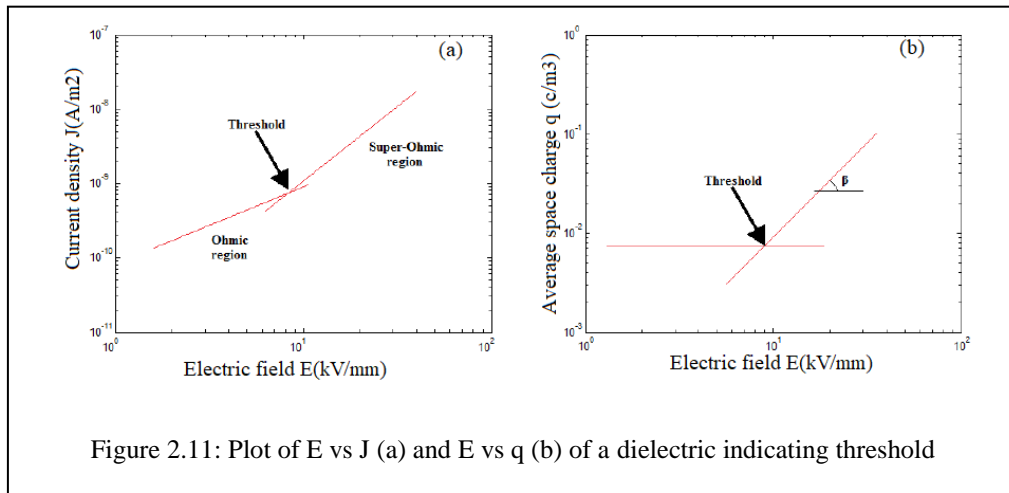
2.4 Electric field threshold for space charge accumulation

For a given insulation, it can be thought that depending on the mechanisms that induce aging, different threshold levels can exist. For example, the threshold for electrical treeing, the value of the electric field that can trigger microscopic damage, induce partial discharges in cavities and to trigger electrical trees. Similarly, the threshold for space charge formation that can degrade the insulation can be thought of [16].

At lower electric field values, the positive and negative charge carrier concentration in the insulating material is equal, a linear relationship exists between the current density and applied electric field. It follows an ohmic behaviour. As the electric field is increased, a shift from ohmic to super-ohmic or high field behaviour is observed. The value of electric field at this transition is the threshold for space charge accumulation.

The threshold value can be estimated either by conduction current measurements or space charge measurements. Both methods should give very close electric field threshold values [16]. The threshold value depends strongly on the temperature. It decreases as the temperature is increased, probably because injection from electrodes is prompted by high temperature. The value also depends on the material of the electrode and the type of interface with the electrode material.

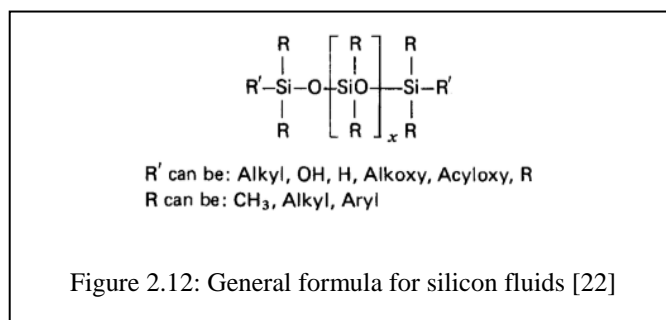
The threshold value can be estimated from the plot of electric field vs current density (E vs J) from conduction current measurements on log-log scale. It can also be calculated from the plot of average space charge density (E vs q) (equal to the integral of space charge density in the sample divided by its thickness) in the insulation vs electric field as shown in figures-2.11 (a) and 2.11 (b).



The electric field threshold and the slope E vs J or E vs q after the threshold value can be used to characterize the insulation material. Since operating at electric fields below the threshold means suppression of formation of space charges. And the equipment can have long life provided no other significant aging mechanisms occur.

2.5 Polymeric structure of silicon insulation

Silicones more accurately called polymerised siloxanes or polysiloxanes are made from the polymerisation of siloxanes with an inorganic chain of silicon and oxygen atoms and are frequently combined with carbon or hydrogen or both or with reactive groups like OH, H, Alkoxy, etc [22]. The chemical formula for silicones can be given as



where R is an organic group such as methyl, ethyl, etc., R' a reactive or non-reactive group as mentioned earlier, and x is the polymerisation index. By varying the -Si-O- chain length (x), side groups (R or R') and crosslinking, silicones can be synthesised with a wide variety of properties.

Silicones are stable, non-reactive and resistant to extreme environments and temperatures from -55°C to +300° C while still maintaining its useful properties like thermal conductivity, fire resistance, dielectric strength, etc. It is because of these properties; silicon fluids are used in traction transformers and in increasingly compact transformers where higher temperatures are expected [23].

These silicones are of three types: 1. Straight chain silicones, 2. Cyclic silicones, 3. Crosslinked silicones. The most common siloxane is linear polydimethylsiloxane (PDMS) commonly known as silicon oil. It is derived by the hydrolysis of dimethyldichlorosilane. The dichloride reacts with water as follows:



The liquid form can be converted to solid state by the process of curing, vulcanization or catalysation. One way of curing this is by condensation i.e. by means of addition of the water molecule. This can be done by exposing the silicone to ambient humidity (water) at room temperature that results in the hydrolysis which continues until the system is fully cured. This method of exposing it to moisture has been employed in this thesis to cure the insulation material.

The chemical formula for the considered silicon insulation material has not been included because of the Patent rights of Lovink Eneritech B.V. This insulation, which is liquid in state is a type of room-temperature vulcanization-1 silicon system. It reacts with the moisture content and gets cured (solidifies).

2.6 Summary

In this chapter, various processes related to charge trapping, injection/extraction and conduction are explained. These are the simplified theoretical models derived from the knowledge of semiconductor physics. They are not very accurate for polymers but are good enough to understand the basic processes involved in charge trapping, injection/extraction and conduction in polymers.

Various parameters related to these principles that can be used for the DC characterisation of the insulation materials can be given as:

- DC conductivity and its dependence on electric field and temperature
- Electric threshold value for space charge accumulation
- Average charge density present in insulation
- Charge distribution in the specimen
- Depletion rate of accumulated charges

The next chapter explains the conduction current measurement and space charge measurement principles. These experiments are performed to determine the conductivity and its dependence on electric field and temperature and electric field threshold values for the silicon insulation.

3. Experiments and Simulation

In this chapter, the test samples, test techniques and experimental setup are explained. In the initial part of chapter, the samples for tests are explained. Later, the principle of conduction current measurement is explained. The space charge measurement principle is described in section 3.3 followed by the pulsed electroacoustic method description and its detailed application for this study. In the last section, the data used for simulation is described.

3.1 Sample preparation and electrode material

In this study, conduction current and space charge measurements are performed on silicon insulation in solid (cured) as well as liquid state. The conduction current measurements are performed at 20°C, 40°C and 60°C. To save time, Space charge measurements using pulsed electro-acoustic method are performed at 20°C alone to verify the electric field threshold value obtained from conduction current measurements at same temperature. An overview of the tests can be listed out as shown in figure-3.1 below.:

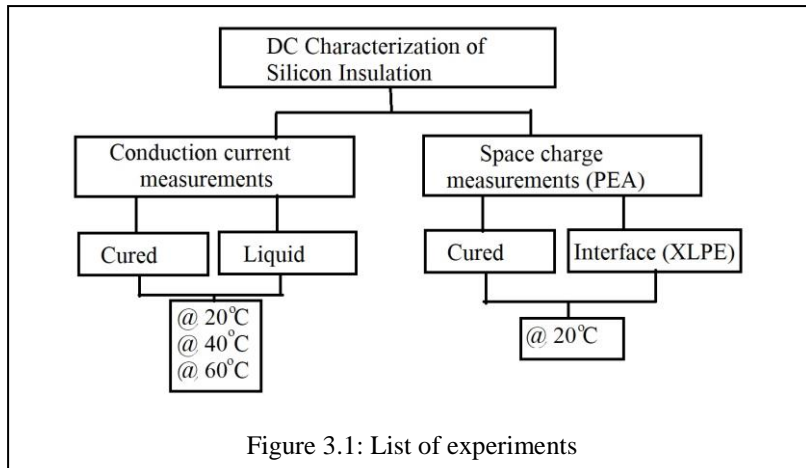


Figure 3.1: List of experiments

This silicon insulation has a property of reacting with the moisture content to change its state from liquid to solid at room temperature. To avoid this reaction, the liquid insulation is stored in an air tight container. An air tight test cell made from aluminium and Teflon was designed and fabricated for containing this insulation during the experiments as shown in figure-3.2.

For the solid sample, liquid insulation of suitable mass (calculated from the density and volume of required thickness) was cured in a Teflon mould. The liquid insulation was exposed to moisture in a humidified chamber at 20°C and 90% humidity for 24 hours. Considering the actual condition at the installation location of cable joint, no special cleaning of these samples was performed. Figure-3.3 below shows the liquid silicon insulation poured into the Teflon mould and the cured silicon insulation sample.

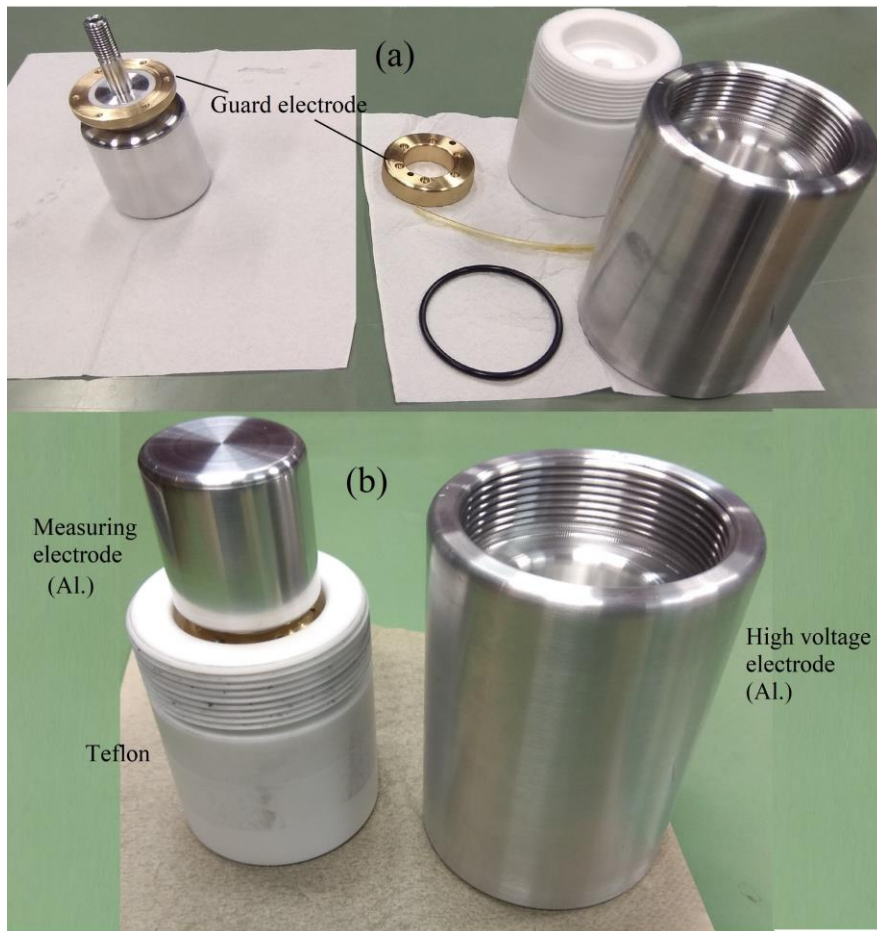


Figure 3.2: Air tight test cell for liquid silicon insulation (a) disassembled (b) assembled

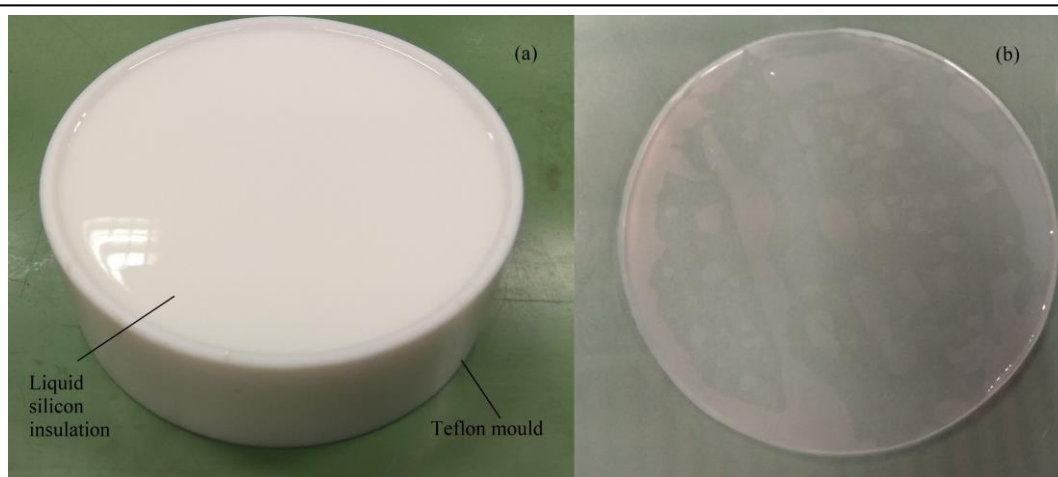


Figure 3.3: Test samples (a) Liquid silicon insulation poured into Teflon mould (b) Cured (solid) silicon insulation sample

Electrode material plays a significant role in the development of space charge in a dielectric [24,25]. To provide electrode-dielectric interface condition that exists in a real cable joint, an aluminium electrode without any semi-conductive layer was used for the conduction current measurements. However, in case of pulsed electro-acoustic method, the acoustic mismatch between the aluminium electrode (high voltage) and silicon insulation resulted in the reduction of the acoustic energy that travels through the dielectric. The remaining acoustic energy got attenuated completely in the dielectric. To reduce this mismatch, a layer of semi-conductive tape is introduced between the high voltage electrode and the dielectric.

The samples used for these experiments are free of charges. For discharging the accumulated space charges in the samples during the experiments, the samples were short circuited, and the temperature was raised to 40°C and this configuration was left for overnight.

3.2 Conduction current Measurements:

The measurement of DC current is useful for two main purposes.

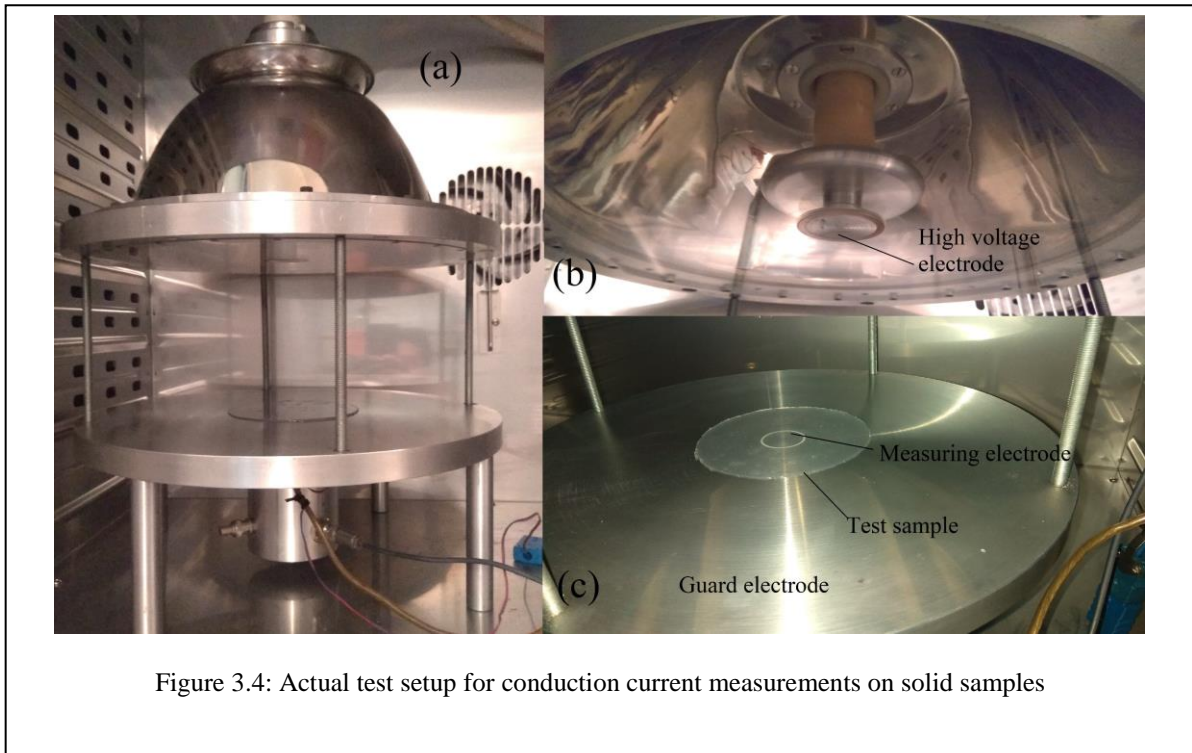
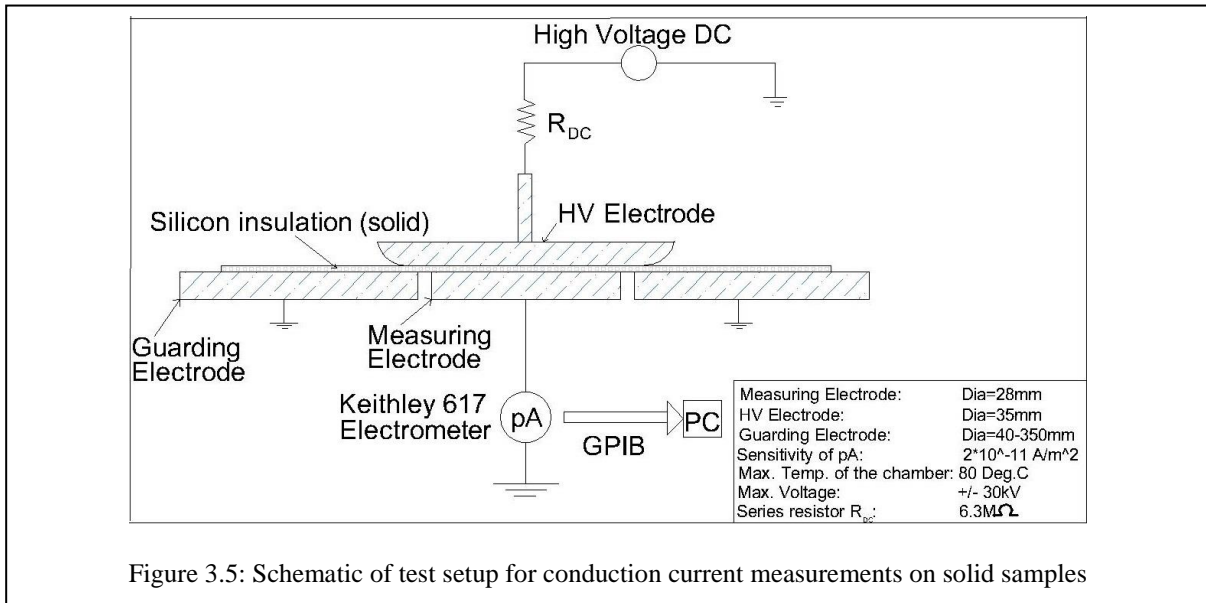
- 1) The DC conductivity of the insulation can be inferred from these conduction current measurements performed at low electric field values where ohmic conduction takes place as explained in section 2.3.3.d. Also, the conductivity dependence on the temperature and electric field can be determined from these measurements.
- 2) An electric field threshold for the onset of space charges in the dielectric can be determined from the plot of voltage-current (or electric field-current density) characteristics as mentioned in section 2.4.

3.2.1 Test setup

Conduction current measurements were performed in a three-terminal cell. A three-terminal cell comprises of a high voltage electrode, measuring electrode and a guard electrode. The guard electrode intercepts all stray currents that otherwise may cause errors. A uniform electric field is maintained between the high voltage and measuring electrode. The entire test setup is shielded completely.

A Keithley 617 electrometer was used for the measurement of the DC current (in the range of pico-amperes). The DC voltage was supplied through a series resistor to protect the electrometer from over currents. Aluminium electrodes were used to simulate an interface that exists in a real cable joint. The profile of electrodes is made as Rogowski profile to avoid the sharp edges where field concentration may occur.

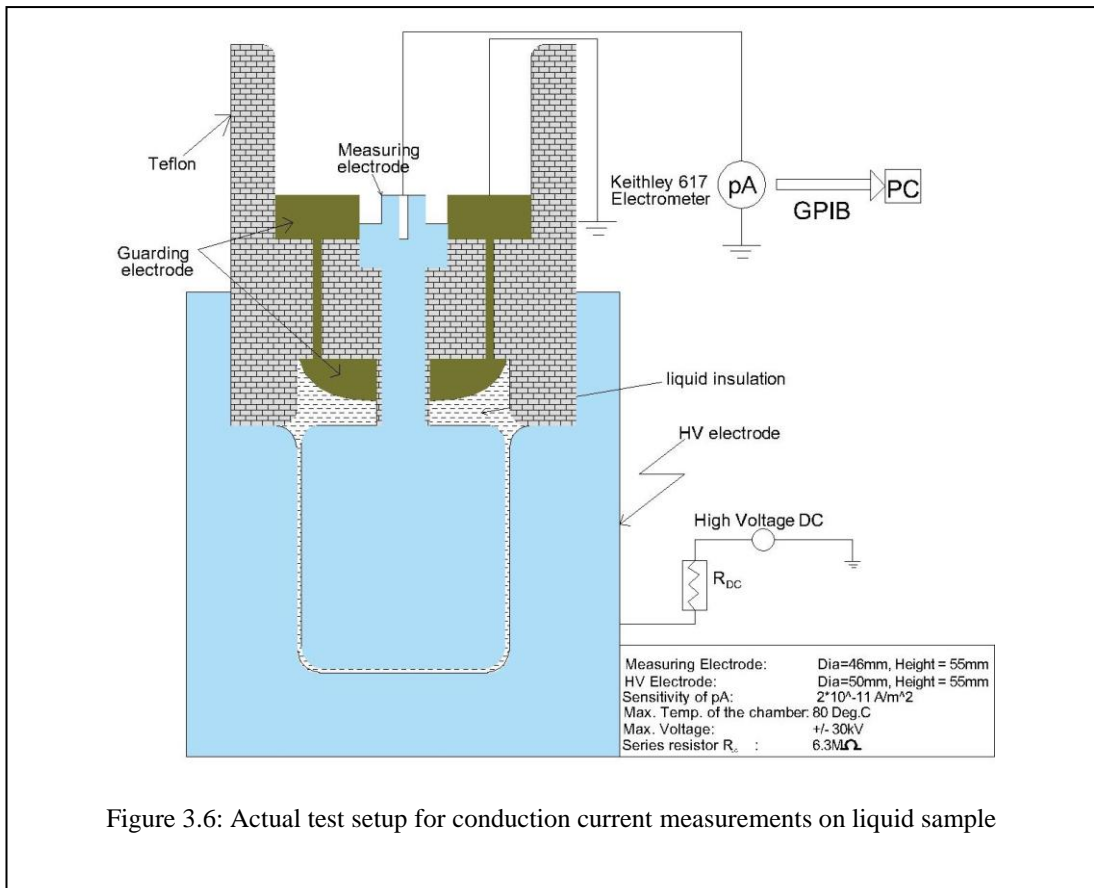
A personnel computer equipped with a GPIB interface was used for displaying and storing the acquired data. A schematic drawing and actual setup for the conduction current measurements on solid samples are shown in figures-3.4 and 3.5 respectively. Figure-3.2 represents the test cell designed for performing conduction current measurements on liquid sample. A schematic representation for this test cell is shown in figure-3.6. Guard electrode in this test cell is designed to reduce the leakage current due to surface discharge (if any). The position of this guard electrode with respect to the measuring electrode might introduce some error into the measurement because of the edge effect. Since, the current due to this edge effect is of much lesser magnitude than the measuring current, this error is neglected.



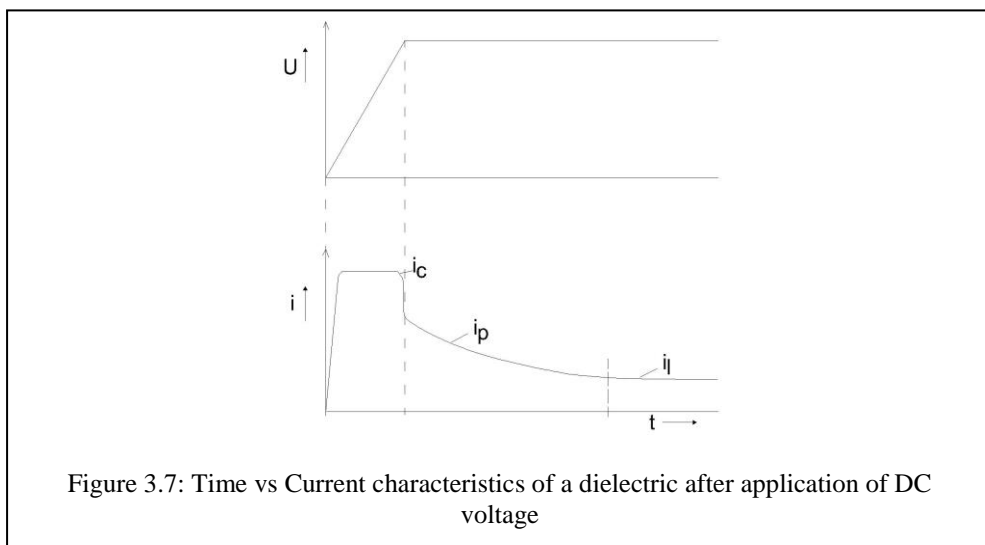
3.2.2 Test procedure

When a DC voltage U is switched on, the dielectric is initially stressed as if the voltage were AC. A capacitive current i_c runs through the dielectric as:

$$i_c = C \frac{dU}{dt} \quad (3.1)$$



After this, a transient phenomenon takes place, where a current i_p called as “polarisation current” or “absorption current” runs through the dielectric. This current decreases slowly and it may take minutes, sometimes hours depending on the material characteristics, temperature, electric field, etc. before a static current i_l is established. This entire process is shown in figure-3.7.



In the low electric field region, the voltage and the static leakage current (i_l) obeys Ohm’s law as explained in section 2.3.3.d. This relation in terms of system properties current density (J) and electric field (E) can be given by,

$$J = \sigma E \quad (3.2)$$

$$J = \frac{i_l}{A_m} \quad (3.3)$$

Where, σ is the conductivity of the insulation and A_m is the area of measuring electrode.

The conductivity of the insulation can be found from equation 3.2 at low electric field values.

To determine the conductivity dependence on temperature and electric field, the experiments were performed at different values of electric field (1 kV/mm to 10 kV/mm for solid and 0.1 kV/mm to 5 kV/mm for liquid silicon insulation) at different temperatures (20°C, 40°C and 60°C).

3.3 Space Charge Measurements

The presence of charges in the dielectric distorts the initial Laplacian electric field distribution that can cause significant field enhancement. Therefore, the magnitude, location and polarity of space charge in a dielectric is a matter of major importance. The conduction current measurements provide an electric field threshold for the onset of space charges in a dielectric without giving any information regarding the distribution of these charges. Space charge measurement techniques can be employed for this.

The space charge measurement techniques provide following information:

- a. Magnitude, Polarity and location of the trapped charges
- b. Electric field threshold value
- c. Electric field can be derived from the measured space charge profile in the dielectric
- d. Results of the measurements can be used for comparing different dielectrics based on their tendency to accumulate charges.

In earlier days, destructive techniques like field mills, capacitive probes and use of powders were employed for the measurement of surface charges. These methods required the test objects to cut into slices to arrive at the site of the charge. This problem was overcome in the following years when non-destructive methods have been employed. The non-destructive methods can be grouped into thermal, acoustic and optical methods.

3.3.1 Thermal group

In the thermal group, a thermal gradient is applied across the sample. The main methods belonging to this group are the Thermal Pulse Method (TPM), the Thermal Step Method (TSM) and the Laser Intensity Modulation Method (LIMM). The way in which the thermal gradient is applied to the sample differentiates these methods. In TPM, the thermal gradient is applied by a flash of light, in TSM it is applied by means of a thermal diffuser. In case of LIMM, a laser beam is used to apply the thermal gradient. The electrical response because of this thermal gradient is measured. This response carries the information about the charge distribution in the sample.

3.3.2 Acoustic group

The most important methods in this group are Pulsed Electroacoustic (PEA) and Pressure Wave Propagation (PWP). Both the methods use the same physical principle based on the acoustic wave propagation through the test sample. The acoustic pressure wave is generated in different ways for these different methods. In PEA, the pressure wave is generated from inside the sample while it is generated outside the sample in case of PWP. The mechanical perturbation caused by this pressure wave in the sample is converted to an electrical signal. This signal contains the information about spatial distribution of charges in sample.

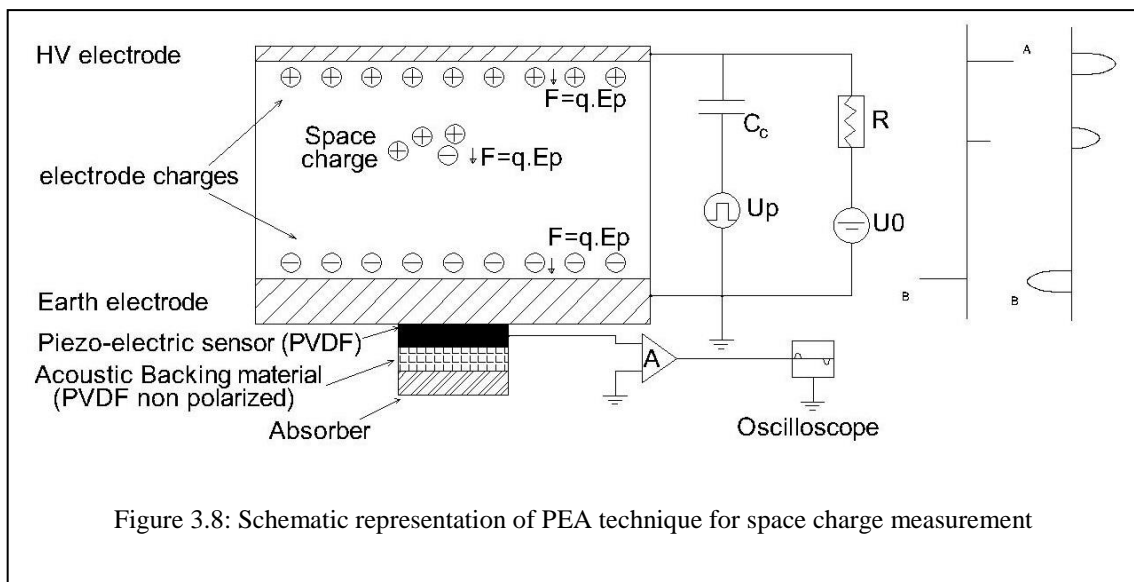
3.3.3 Optical group

The optical methods measure the electric field distribution in the sample (which is transparent) to measure the distribution of charges in it. These methods are based on the Kerr effect and Pockels effect. Kerr effect is used to evaluate the accumulation of space charges in liquid dielectrics whereas Pockels effect is most commonly used to measure the surface charges.

Review of these methods has been done in [26,27]. In This work, pulsed electroacoustic method (PEA) is used.

3.3.4 General theory behind the Pulsed Electro-acoustic (PEA) method

Pulsed Electro-acoustic method is a commonly used non-destructive technique for investigating space charges [12,27]. This method provides the possibility of observing the space charge profile in the insulation bulk. Electric field profile can then be deduced from the space charge distribution. Schematic representation of the PEA technique is shown in figure-3.8.



When a dielectric with trapped charges is placed between the electrodes, charges are induced on the electrode surfaces. This way, even without the application of DC voltage, a spatial distribution of charges arises in the system.

On the application of DC voltage across a charge free dielectric, surface charges are formed at the electrodes, given by:

$$\sigma_{el} = \epsilon \cdot E \quad (3.4)$$

In this method, a pulsed voltage U_p is externally applied to the dielectric along with the DC voltage U_0 . The pulsed electric field induces a perturbation electric force on each charge in the sample. This force causes the charge to move slightly in its position. This movement launches an acoustic pressure wave $p(t)$ that travels in either direction from the charge location. This transient pressure wave will have an amplitude proportional to the local net charge density and its arrival time at the sensor contains information about the position of the charges. A piezoelectric sensor is used to detect the acoustic wave and transform the acoustic wave into an electrical signal. Thus, the charge distribution inside the sample becomes accessible by this electrical signal processing. This signal is then fed to an oscilloscope after amplification for detection and data storage. Depending on the properties and thickness of the sample, the amplitude of the pulse ranges between 0.1 kV to 4 kV and pulse width varies from 5ns to 200ns.

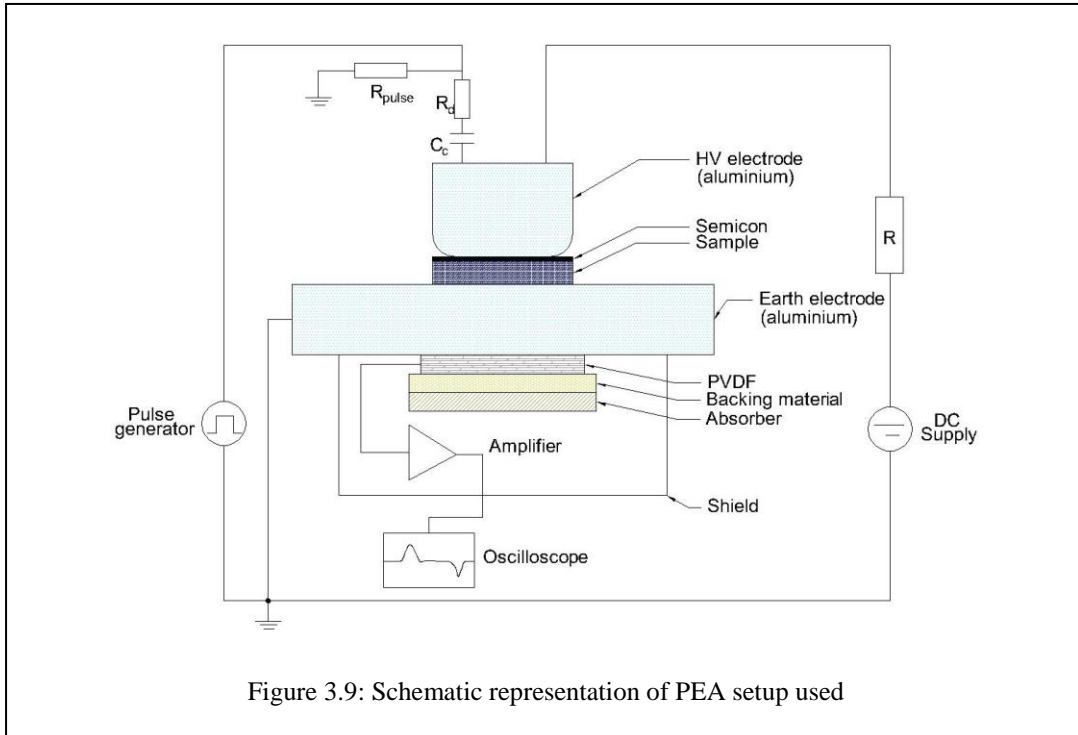
A thick earth electrode is used in this method. In this way, the earth electrode delays the acoustic wave reaching the piezoelectric sensor. This delay is necessary, because of the interference of the electromagnetic noise caused by the firing of pulse. Further an acoustic backing material (with same acoustic impedance as that of piezoelectric material) and absorber are used to minimise the reflection of signal due to acoustic mismatch.

In principle, with a very high resolution, the surface charge densities at the electrodes should be delta functions if expressed in coordinates of volume space charge density. However, because of the finite resolution of the measurement system and a finite width of the applied voltage pulse, it is not possible to obtain this ideal result.

The amount of space charge in the bulk of the sample can then be calibrated by applying a voltage low enough to not to inject any charges which results in a known amount of electrode charge.

3.3.5 Pulsed Electro-acoustic method for thin plaques

A representation of the schematic for the PEA test setup used is shown in figure-3.9 with an actual PEA table in fig. 3.10. The electric pulse is generated by a pulse (80ns) generator. An HVDC supply is used to apply DC electric field to the sample during measurement. A piezoelectric sensor of 9 μ m detects the acoustic pressure wave to convert it into an electric signal.

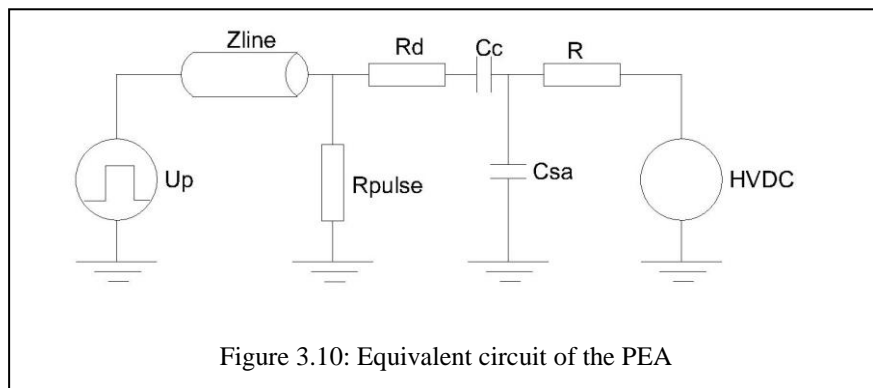


The specifications of the PEA test setup are given in table 3.1.

Table 3.1 Specifications of the PEA setup used

PEA setup for flat specimens	
Amplifier	Gain = 75 dB Input impedance = 50 Ω Bandwidth = 30 kHz – 955 MHz
Sensor	PVDC, 9 μ m
Pulse generator	Amplitude = 0-2 kV Pulse width = 80 ns

The equivalent circuit for the signal path in PEA can be shown as in figure-3.11. The input impedance R_d is 157 Ω , the termination resistance R_{pulse} is 50 Ω , which is equivalent to Z_{line} , to properly terminate the pulse transmission line.



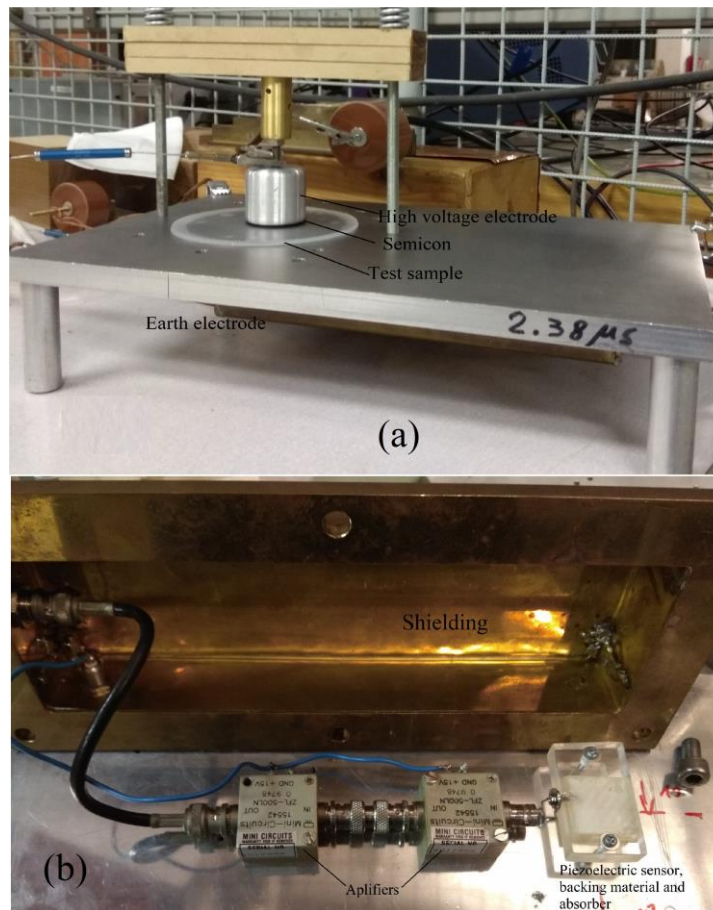


Figure 3.11: Actual PEA setup used (a) Upper part of PEA table (b) Bottom part of PEA table

Acoustic properties of the materials:

Acoustic properties of the materials use are given in table 3.2 below:

Table 3.2 Acoustic properties of the different materials in the PEA setup [28,30]

Material/Property	Density	Acoustic velocity	Acoustic impedance	Relative permittivity
	ρ (kg/m ³)	u (m/s)	$Z = \rho * u$ (kg/m ² s)	ϵ_r
Aluminium	2690	6420	$17.3 * 10^6$	1
Semicon	990	1950	$1.9 * 10^6$	-
XLPE	900	2000	$1.8 * 10^6$	2.3
PVDF – α / β	1780	2260	$4 * 10^6$	13
Silicon insulation - Liquid	978	1010	$9.88 * 10^5$	2.9
Silicon insulation – Solid	971	1000	$9.71 * 10^5$	2.6

PEA setup parameters:

In order to obtain high relative resolution, initially a narrow electric pulse should be selected, and then a thin transducer should be used. However, when the acoustic wave travels through the silicon sample, it gets attenuated. This attenuation is frequency dependant. High frequency components are more attenuated than the low frequency components. To minimise this effect, a pulse of width, $\Delta T_p = 80$ ns is used in these experiments.

a. Relative space resolution:

The space resolution of space charge distribution is mainly determined by ΔT_p of the pulse. This can be given by,

$$r = \frac{\Delta T_p}{d/u_{sa}} \times 100\% \quad (3.5)$$

Where, u_{sa} is the acoustic velocity in the sample.

$$r = 9.5\%$$

A Transducer of thickness 9 μ m is used to minimize the effect of transducer thickness.

b. Coupling capacitor:

The coupling capacitor's main purpose is to isolate the pulse circuit from HVDC circuit. Apart from this, it has two important functions: Firstly, it ensures that most of the DC voltage is applied to the sample. Secondly, if chosen properly, it ensures that most of the pulse voltage appears across the sample [25]. For this to occur, C_c should be much greater than the sample capacitance C_{sa} .

$$V_{sa} = \frac{V_p(t)C_c}{C_c + C_{sa}} \cong V_p(t) \quad (3.6)$$

This condition is satisfied using equation 3.7

$$C_c \geq 100 \times C_{sa} \quad (3.7)$$

Capacitance of the Sample is given by: $C_{sa} = \frac{\epsilon_0 \epsilon_r S}{d}$

Where, S is the area of the HV electrode and d is the thickness of sample.

The permittivity of insulation is 2.6 and thickness 0.85mm and electrode diameter is 40mm

$$C_{sa} = \frac{8.85 \times 10^{-12} \times 2.91 \times 1256 \times 10^{-6}}{0.85 \times 10^{-3}} = 34 \text{ pF}$$

So, the value of pulse power capacitor shall be $\gg 3.4$ nF

c. Series resistance R

The series resistance R is used to make sure that most of the pulse voltage is applied to the sample. It also limits the current in case of breakdown of the sample. The value of this resistance can be find out using equation 3.8:

$$R_{dc} \gg \frac{1}{2\pi f_p C_{sa}} \quad (3.8)$$

$$R_{dc} = 500 * \frac{1}{2\pi f_p C_{sa}} \quad (3.9)$$

Where, f_p is the main frequency component of the pulse which can be calculate using equation 3.10.

$$f_p = \frac{1}{2\Delta T_p} \quad (3.10)$$

With the pulse duration as 80ns, the minimum value of series resistance can be calculated as:

$$f_p = \frac{1}{2 * 80 * 10^{-9}} = 6.25 \text{ MHz}$$

$$R_{dc} = 500 * \frac{2 \Delta T_p}{2\pi C_{sa}} = 0.33 \text{ M}\Omega$$

Measurement Procedure:

Measurements are performed only when the DC voltage is on. This is performed to verify the electric field threshold value. In this case, the space charges which are formed due to the applied voltage are measured along with the surface charges at the electrodes. The electrode surface charge is composed of two values one is because of the applied voltage and the other component is induced by the space charges.

A plot of electric field vs the average space charge density in the sample shows the transition from linear E-Q region to the non-linear E-Q region.

Signal correction:

The electrical signal received at the scope does not directly represent the acoustic signal at the sensor. It is because the sensor-amplifier combination in the system acts as a high pass filter [29]. To correct this detected signal, deconvolution techniques are adopted. The deconvolution process does the following: a transfer function for the entire system is obtained for a signal of known shape. This transfer function is then used to calculate the processed signal from a received signal. This deconvolution in time domain is equivalent to division of output signal by the transfer function in frequency domain.

The dielectric material is mechanically a very lossy media. So, the acoustic waves are attenuated while travelling through the dielectric. This attenuation is seen in the decreasing

amplitude. So, the acoustic signal detected at the sensor does not directly correspond to the space charge distribution in the sample. The original acoustic signal must be recovered from the attenuated signal. This is attenuation is frequency dependant; the high frequency components are attenuated more than the low frequency ones. It results in the broadening of the signal as it travels through the sample.

Calibration procedure:

In order to convert the corrected detected signal [mV] to a space charge density signal, [C/m³], the measuring system has to be calibrated. This can be carried out based on the known amount of charge at the earth electrode on the application of voltage to a charge free sample.

To convert a corrected voltage signal $v_{pr}(t)$ to a calibrated space charge profile $\rho(t)$, a calibration factor k_{cal} can be defined as:

$$K_{cal} = \frac{v_{pr}(t)}{\rho(t)} \quad (3.11)$$

Where, $v_{pr}(t)$ is the signal after deconvolution and attenuation correction.

In order to determine the calibration factor, a DC voltage V of magnitude below the threshold value is applied to a charge free sample. The calibration factor then be calculated as:

$$K_{cal} = \frac{v_{pr}(t)}{\rho_e} \quad (3.12)$$

Where, ρ_e is the earth electrode surface charge density, which, for a known voltage V can be calculated as,

$$\rho_e = \varepsilon_0 \varepsilon_r E_e = \varepsilon_0 \varepsilon_r \frac{V}{d} \quad (3.13)$$

Where, d and ε_r are the thickness and dielectric permittivity of the sample

In order to verify that the calibration is performed correctly, the electric field distribution across the sample can be calculated as per eq. 3.8.

$$E(x) = \frac{1}{\varepsilon_0 \varepsilon_r} \int_0^d \rho(x) dx \quad (3.14)$$

3.4 Cable Joint Simulation

COMSOL Multiphysics (finite element modelling software) is used for simulating the electric field distribution in cable joint under AC as well as DC conditions. 2-D axis symmetric simulations are performed. The cable joint used in simulations is a 12/20 kV (U_0/U) silicon insulation filled straight through joint for polymeric cables as shown in figure-1.1. Geometry of cable joint used in the simulation is shown in figure-3.12.

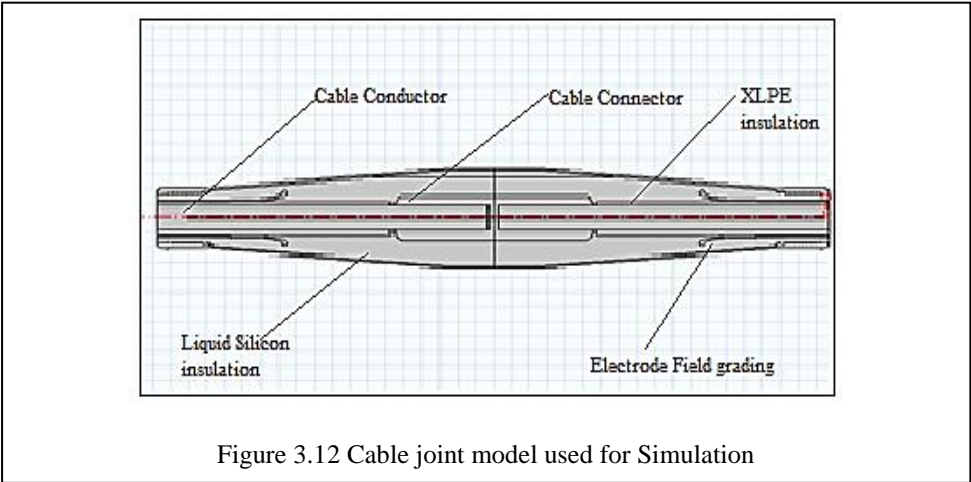


Figure 3.12 Cable joint model used for Simulation

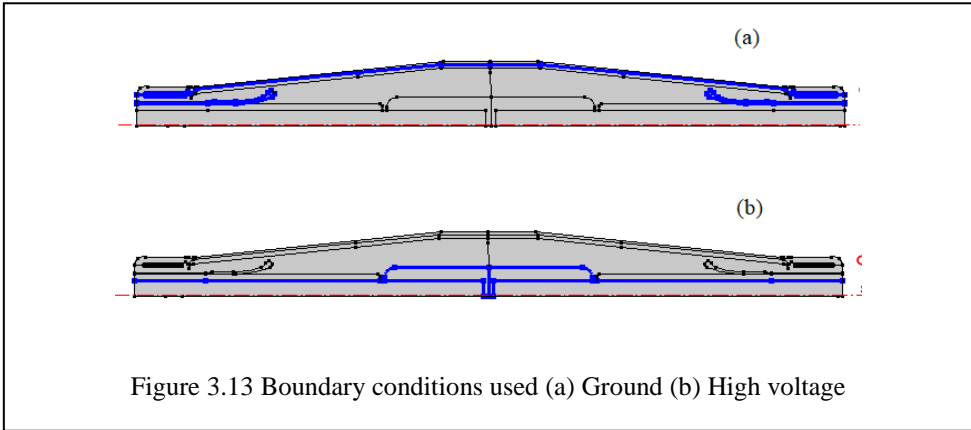


Figure 3.13 Boundary conditions used (a) Ground (b) High voltage

Simulations are performed for following different scenarios in presence of two different temperature gradients of 30°C and 60°C across the cable joint.

1. Cable joint under AC condition
2. Cable joint under DC condition, no curing of silicon insulation
3. Cable joint under DC condition, with presence of cured silicon insulation – Cured silicon layer is considered near the outer screen of cable joint and on the surface of the field grading. The cured silicon layers are highlighted in blue in figure-3.14.

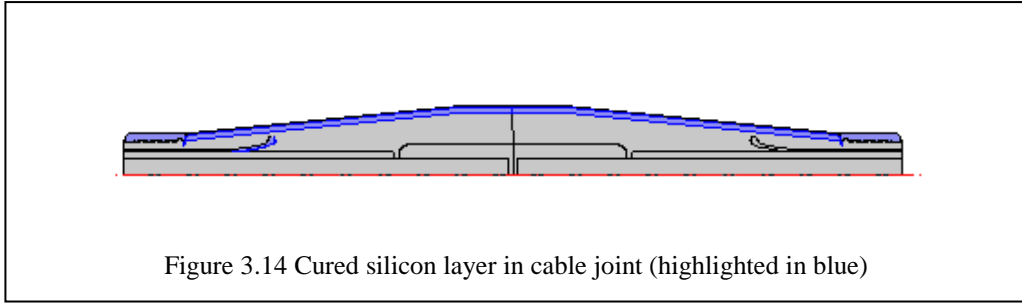


Figure 3.14 Cured silicon layer in cable joint (highlighted in blue)

For the above-mentioned scenarios, the electric field is monitored at different locations in the cable joint. These location are indicated in figure-3.15 by using cut lines.

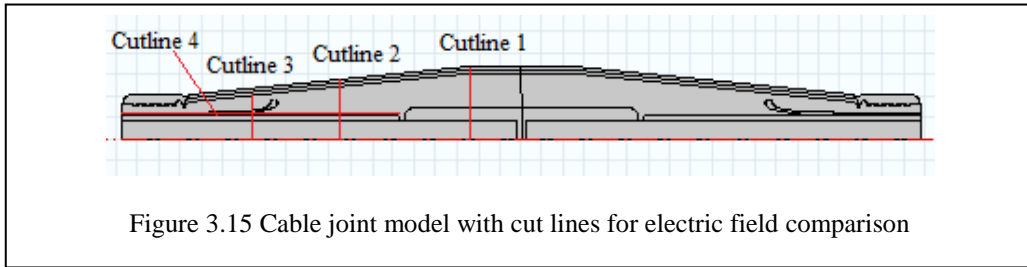


Figure 3.15 Cable joint model with cut lines for electric field comparison

Cut lines 1 to 3 are for observing the normal electric field at these locations. Cutline 4 is for the tangential field observation at the cable insulation surface. The simulation is performed for $U_0=12$ kV under AC. While for DC, U_0 is considered as 17 kV, which is equivalent to the peak of AC rms voltage U_0 .

The temperature at cable conductor is considered as 90°C and the temperature at the outer screen of cable joint is varied to have the gradient of 30°C and 60°C across the cable joint.

The conductivity (σ) for polymeric insulation, is defined in the simulation by an empirical formula given by equation 3.15 [19].

$$\sigma = \sigma_0(\exp(\alpha(T - T_0)))(\exp(\gamma(E - E_0))) \quad (3.15)$$

Where, σ_0 denotes the conductivity of insulation at reference temperature of $T_0^\circ\text{C}$ and electric stress of E_0 kV/mm, α is the temperature dependency coefficient in $1/^\circ\text{C}$ and γ is the field dependency coefficient in mm/kV. For XLPE, α and γ are considered as 0.1 $1/^\circ\text{C}$ and 0.05 mm/kV respectively and the initial conductivity as $\sigma_0 = 1 \times 10^{-16}$ S/m [19].

For the cured silicon insulation, values of σ_0 , α and γ are found from the conduction current measurements. These values are: $\sigma_0 = 1 \times 10^{-16}$ S/m, $\alpha = 0.0523$ $1/^\circ\text{C}$ and $\gamma = 0.224$ mm/kV. These values are calculated from the conduction current measurements presented in the results chapter.

For the liquid silicon insulation, conductivity is considered as a function of temperature only. This is because the conduction mechanism in liquid dielectrics is not fully understood yet. The conductivity values of liquid silicon insulation at different temperatures is given in table 3.3.

Table 3.3 Property of liquid silicon insulation used in simulations

Temperature	Liquid silicon insulation Conductivity σ (S/m)
	At E=0.4 kV/mm
20°C	1.6 E -11
40°C	2.4 E -11
60°C	4 E -11

All other properties for solid silicon insulation are considered similar to those of liquid silicon insulation.

The properties of other materials used in simulations is given in table 3.4.

Table 3.4 Properties of materials used in simulation

Properties	Aluminium core	XLPE insulation	Conductive screen	Liquid silicon insulation	Cured silicon insulation
Relative Permittivity	1	2.25	2.6	2.9	2.6
Thermal Conductivity (W/m. K)	155	0.4	0.5	0.19	0.19
Heat capacity at constant pressure (J/ Kg. K)	893	2200	750	1550	1550
Electrical conductivity (S/m)	3.50×10^7	Eqn. (3.15) with $\sigma_0 = 10^{-16}$, $\alpha = 0.10$, $\gamma = 0.05$	2	T vs σ Plot (table 3.3)	Eqn. (3.15) with $\sigma_0 = 10^{-16}$, $\alpha = 0.05$, $\gamma = 0.22$
Density (Kg/m³)	2730	823	1110	980	980

3.5 Summary

The preparation of test samples, test techniques, test setups and simulation data are explained in this chapter. The experimental results and the discussion are presented in the next chapter.

4. Experimental results

In this chapter, results of conduction current and space charge measurements using PEA are presented and discussed. Section 4.1 contains the results related to conduction current measurements on cured as well as liquid silicon insulation. In section 4.2, the results of space charge measurements on cured silicon insulation samples are included. Results of simulations performed on the silicon filled cable joint are presented in section 4.3.

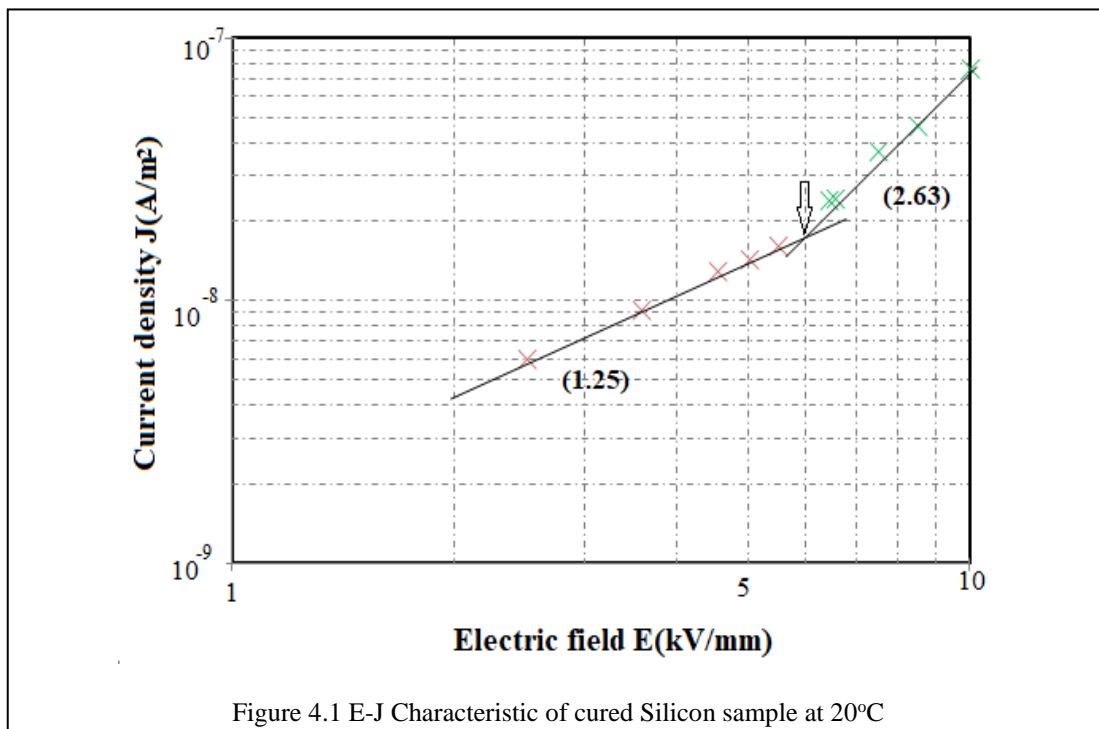
4.1 Conduction current measurements

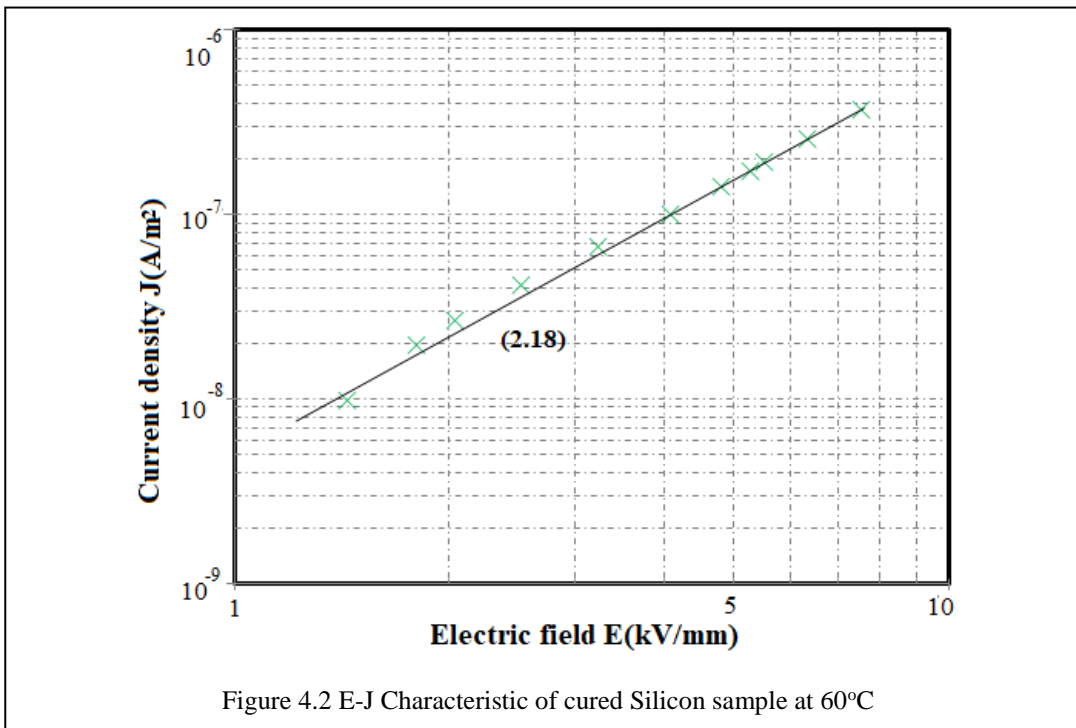
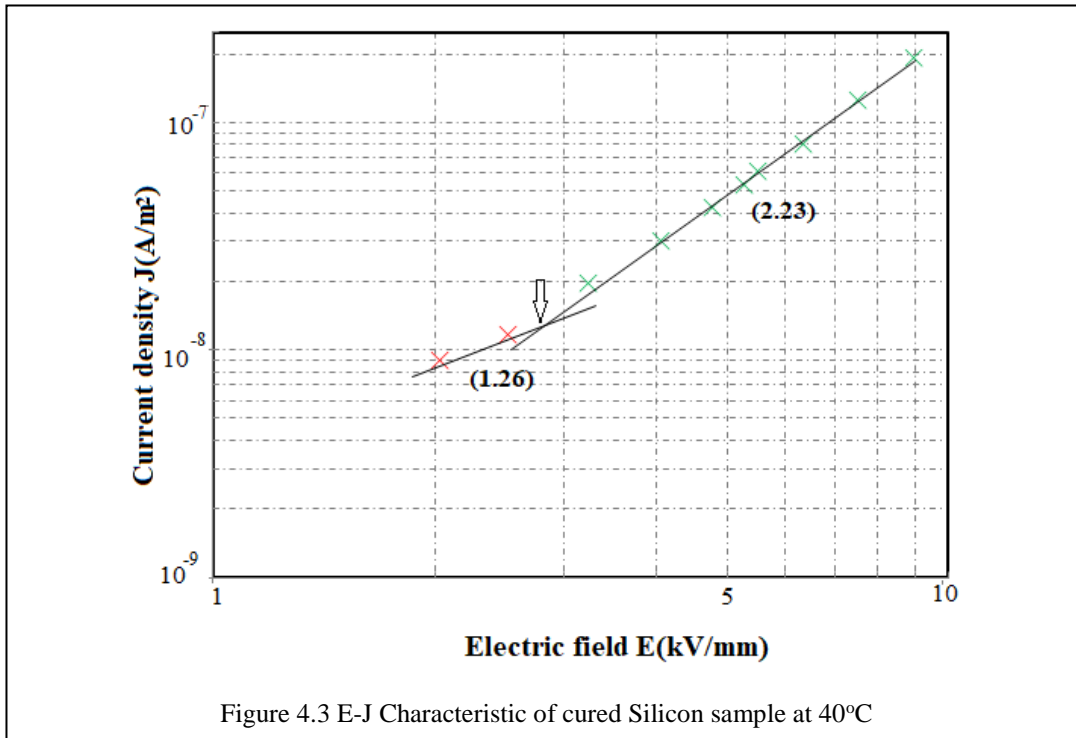
Conduction current measurements have been carried out at different electric field values between 0.2 kV/mm to 10 kV/mm. Temperature was varied in the steps of 20°C, 40°C and 60°C.

The electric field thresholds of the cured samples at different temperatures were evaluated via the electric field-current density characteristics as explained in section 2.4. Below the threshold value, the voltage-current relationship is ohmic and the conductivity is constant. In the super-ohmic regime, the conductivity increases with electric field.

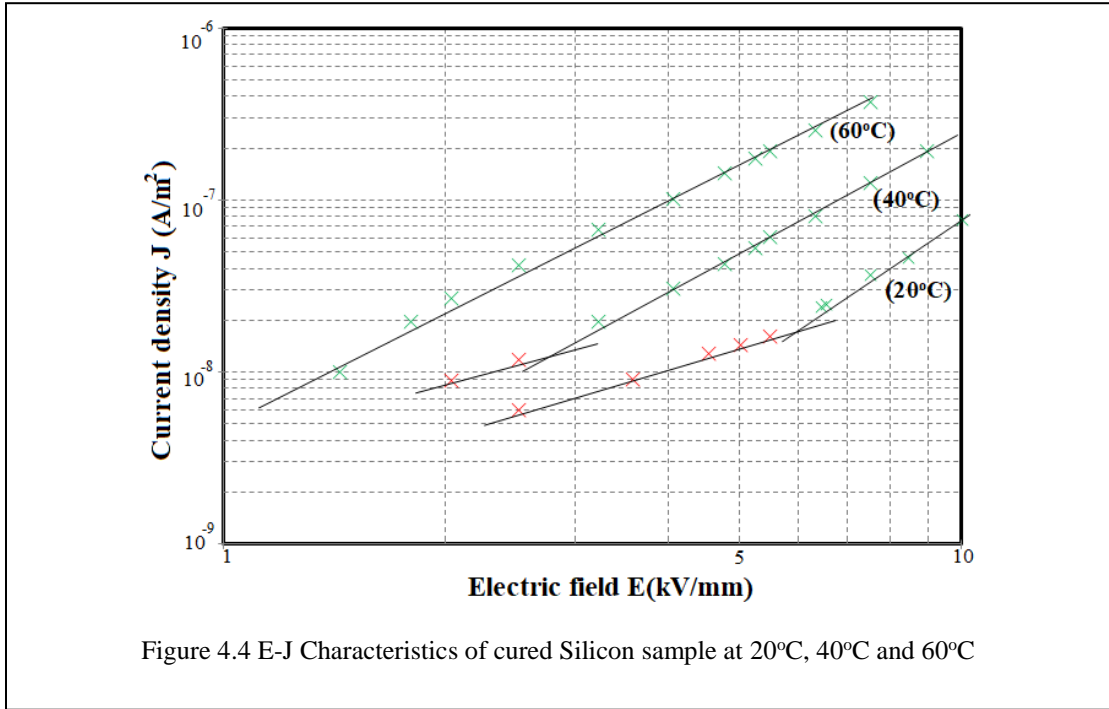
4.1.1 Cured (solid) silicon insulation

The electric field threshold at which conduction mechanism changes from ohmic to super-ohmic regime at 20°C, 40°C and 60°C is indicated by an arrow in the figures-4.1, 4.2 and 4.3 respectively. The slope of the regression lines on these plots is indicated in brackets. The transition from ohmic to super-ohmic region can also be observed from the change of the slope.

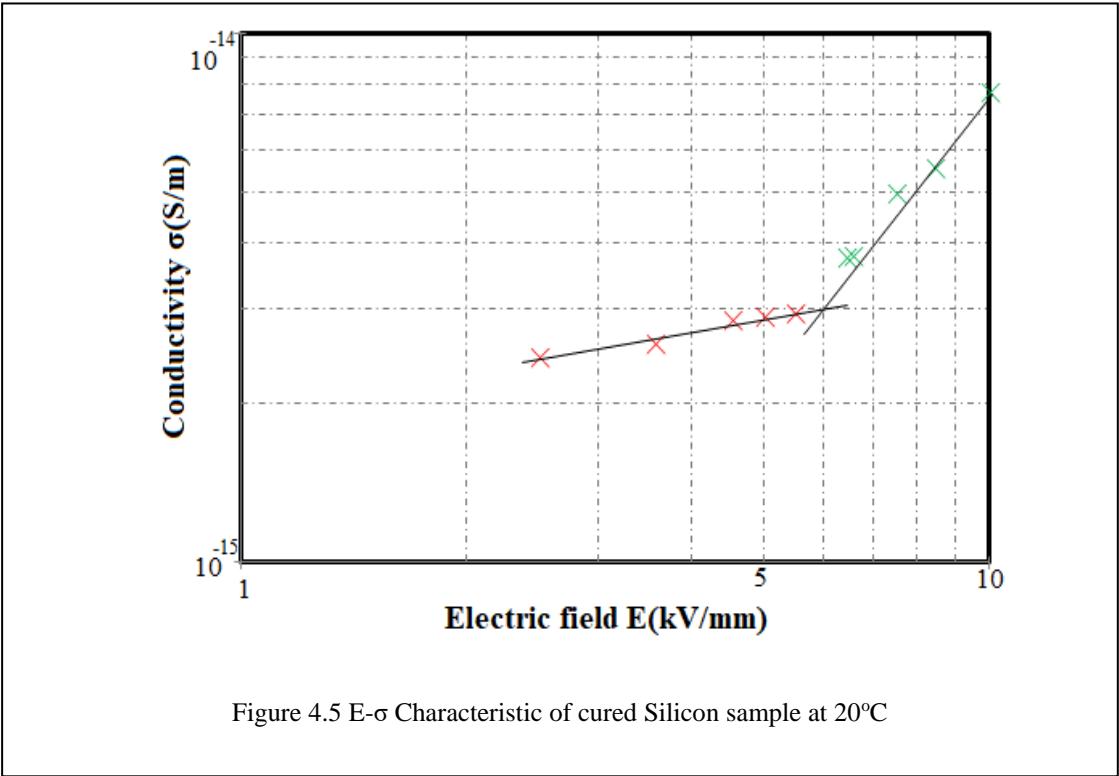




A combined plot of the electric field vs current density characteristics at 20°C, 40°C and 60°C is shown in figure-4.4 below.



At 20°C, the electric field threshold is found to be at 6 kV/mm. At 40°C the threshold value is lowered to 2.7 kV/mm. And at 60°C, no ohmic region is found. The electric field (E) – conductivity (σ) characteristics for this sample are presented in figures 4.5 to 4.7.



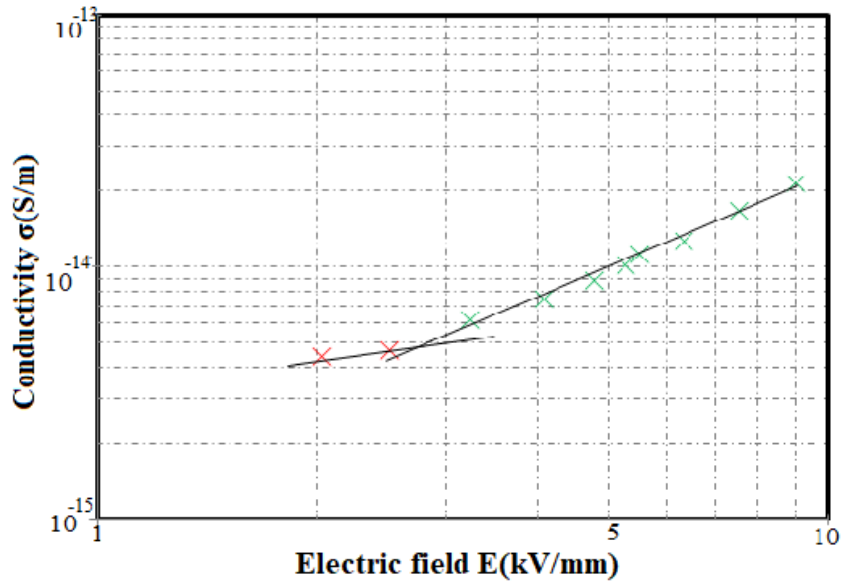


Figure 4.6 E- σ Characteristic of cured Silicon sample at 40°C

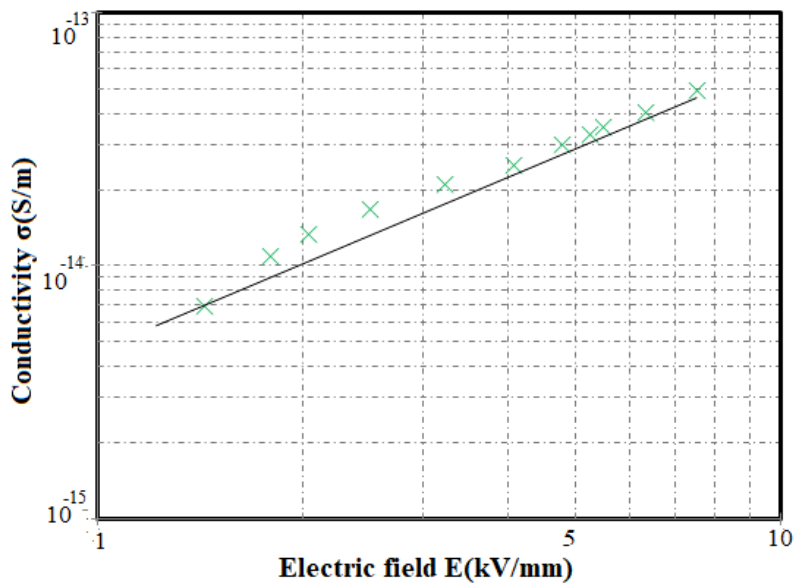
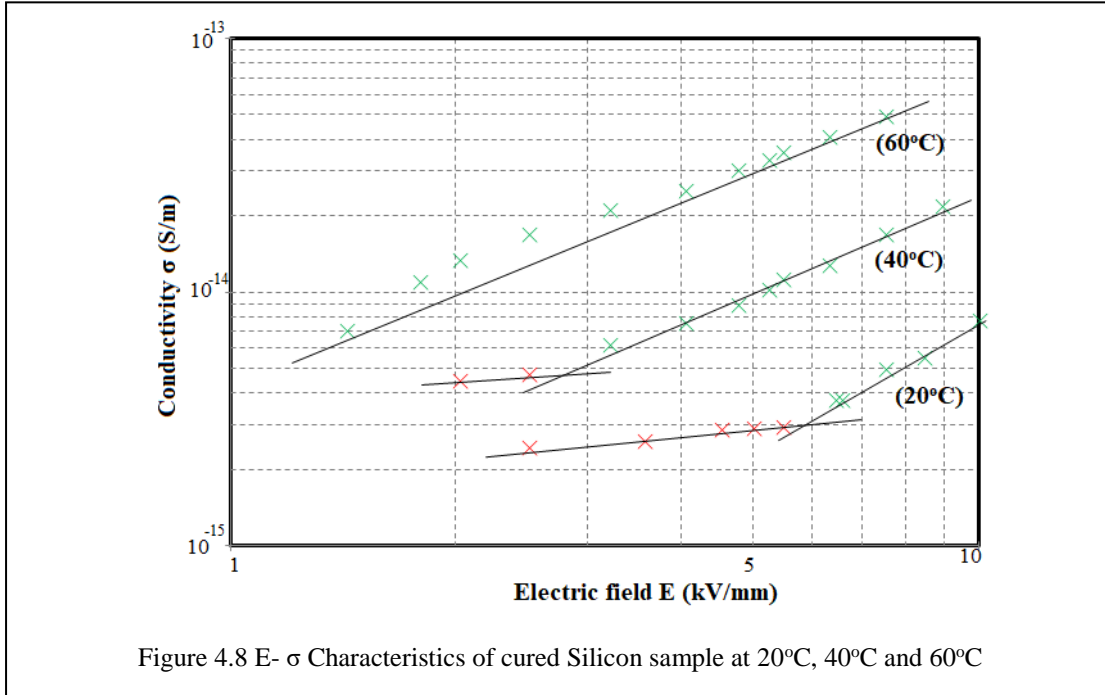


Figure 4.7 E- σ Characteristic of cured Silicon sample at 60°C

A combined plot of electric field vs conductivity characteristics at 20°C, 40°C and 60°C is shown in figure-4.8.



At 20°C and 40°C, the conductivity of the cured silicon sample can be calculated by averaging the conductivity values in ohmic region while at 60°C, it is the value at the required reference electric field. As expected, the conductivity increases with increase in temperature, showing positive temperature coefficient behaviour.

Equation 3.15 is an empirical formula for the electric field and temperature dependant conductivity of polymeric insulation materials. For the cured silicon insulation, a similar expression can be followed. The electric field and temperature dependency coefficients calculated from the conduction current measurements are given in table 4.1.

Table 4.1 Electric field and temperature dependency coefficients

	In ohmic regime @ 2.5 kV/mm	In super-ohmic regime @ 7.5 kV/mm
α ($^{\circ}\text{C}$)	0.0483	0.0576
γ @ 20°C (mm/kV)	0.0677	0.197
γ @ 40°C (mm/kV)	0.113	0.224
γ @ 60°C (mm/kV)	-	0.299

From the plots, it is also observed that the conductivity of cured silicon insulation at a given field of 2.5 kV/mm and within the range of 20°C and 60°C, fits well with an Arrhenius-type relationship.

$$\sigma(T) = A e^{\left(\frac{-B}{T}\right)} \quad (4.1)$$

Where, A is the pre-exponential constant and B is the constant for activation energy for conduction.

The values of constants A and B calculated from figure 4.9 are:

$$B = 4.68 \times 10^3 \text{ K}$$

$$A = 1.89 \times 10^{-8} \text{ S/m}$$

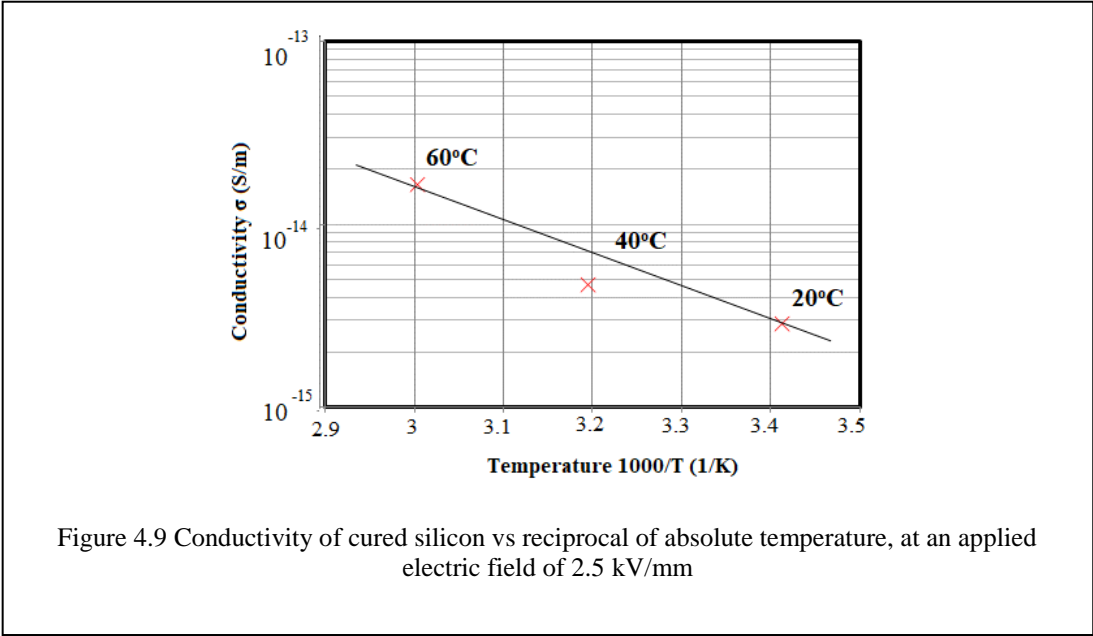
The corresponding activation energy for cured silicon insulation is 0.4eV. This value is 1/4th of the activation energy of XLPE as reported in [30].

Electrical conductivity in a dielectric can be given by:

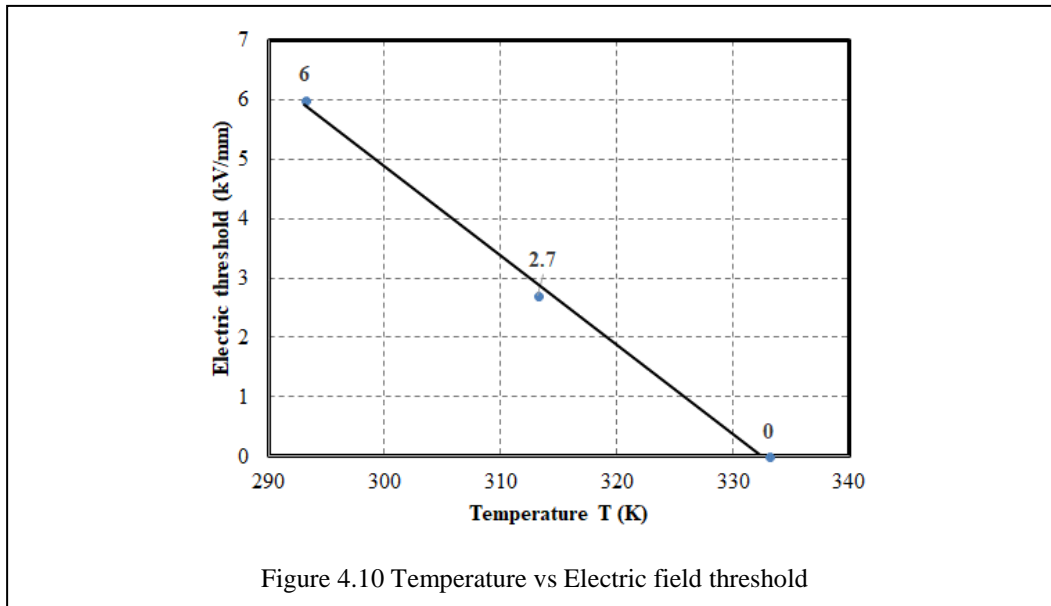
$$\sigma = ne\mu_n + pe\mu_p \tag{4.2}$$

Where, n and p represent the charge carrier concentration and μ_n and μ_p represent the mobilities of negative and positive charge carriers respectively. And e is the charge on single charge carrier ($1.6 \times 10^{-19} \text{ C}$).

As explained in section 2.3.3.d, although not all charge carriers contribute to conduction, e.g. due to trapping, this effect is rather limited as Arrhenius-type behaviour is followed quite closely. This can be attributed to the fact that the charge carrier concentration and the mobility follows an Arrhenius-type behaviour with the temperature.



The electric field threshold follows an inverse relation with temperature. This relation is plotted in figure-4.10.



4.1.2 Liquid Silicon insulation

The various international standards available for measurement of conductivity or resistivity of insulating liquids are given in table 4.2.

Table 4.2 Standards for measurement of conductivity or resistivity of insulating liquids

Standard	IEC 61620	IEC 60247	ASTM D1169
Title	Insulating liquids – Determination of the dielectric dissipation factor by measurement of the conductance and capacitance – Test method	Insulating liquids – Measurement of relative permittivity, dielectric dissipation factor ($\tan \delta$) and DC resistivity	Standard Test Method for Specific Resistance (Resistivity) of Electrical Insulating Liquids
Method	Current measurement, trapezoidal voltage	Current measurement, DC voltage	Current measurement, DC voltage
Electric field strength	≤ 0.1 kV/mm	≤ 0.25 kV/mm	0.2 to 1.2 kV/mm
Time of energization	0.4 - 5 s (trapezoidal square wave, $f = 0.1$ to 1 Hz, rise time 1 to 100 ms)	1 min	1 min direct polarity / 5 min short circuit / 1 min reversed polarity

As indicated in table 4.2, the available standards propose the measurement of DC conductivity of insulating liquids at low electric field values and at lower energization time. The reason is that the thermodynamic equilibrium in the liquid will not be disturbed significantly at such values. Based on this, the commercially available test cells are designed and hence are not suitable for high electric field measurements.

In liquid dielectrics, both the current density and conductivity are time-dependant. This is due to the ion drift processes in the dielectric as shown in figure-4.11.

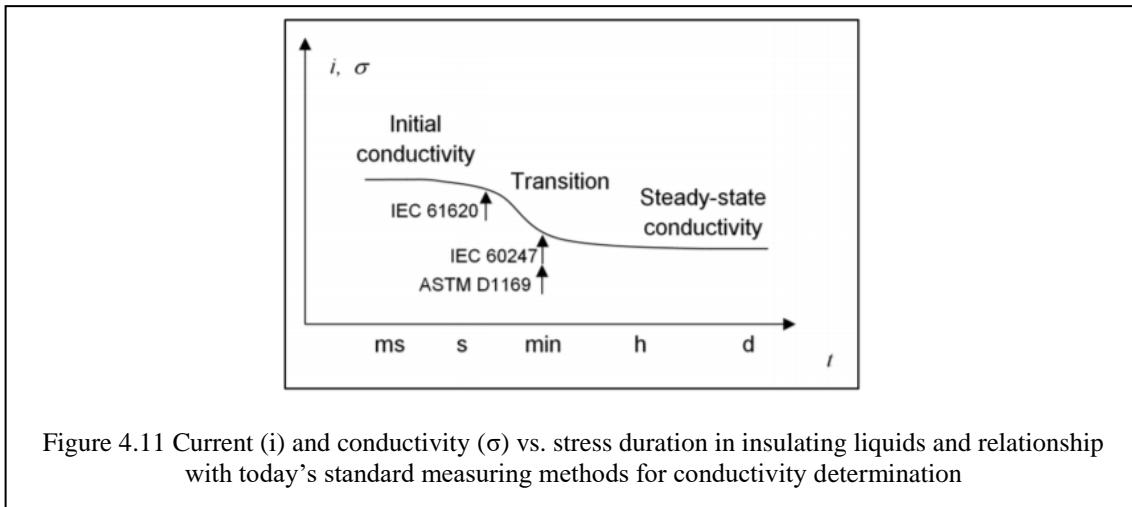


Figure-4.11 indicates that the conductivity and its behaviour observed at an early instant of energization time is normally completely different from steady state behaviour. This is because of the charge carrier drift processes which lasts for longer times and charge injection, generation and recombination processes. In many cases, quasi steady state conditions are reached within 10000s [31]. However, in this study, to be sure of the steady state regime, the current density and conductivity are measured after 24 hours (86000s) of energization time.

In order to apply high electric fields to the liquid insulation, the test cell described in section 2.3 is used. The test cell has been designed to withstand 25 kV DC voltage level, applying 12.5 kV/mm electric field to the insulation. The measurements have been performed at electric fields in the range of 0.1 kV/mm – 5 kV/mm and at temperatures 20°C, 40°C.

On the first sample of liquid silicon insulation, electric fields in the range of 1 kV/mm - 7 kV/mm were applied to observe the current and its behaviour. Figure-4.12 shows a plot of time vs leakage current when the electric field is in the range of 1 kV-7 kV is applied across the sample. It is observed that, at lower values of electric field, the current reaches a quasi-steady state. Whereas, at fields 5 kV/mm and above, variations in the current are observed. It is believed that these variations are the result of movement of charge carriers (ions). A similar phenomenon in mineral oils has been reported in [31,32].

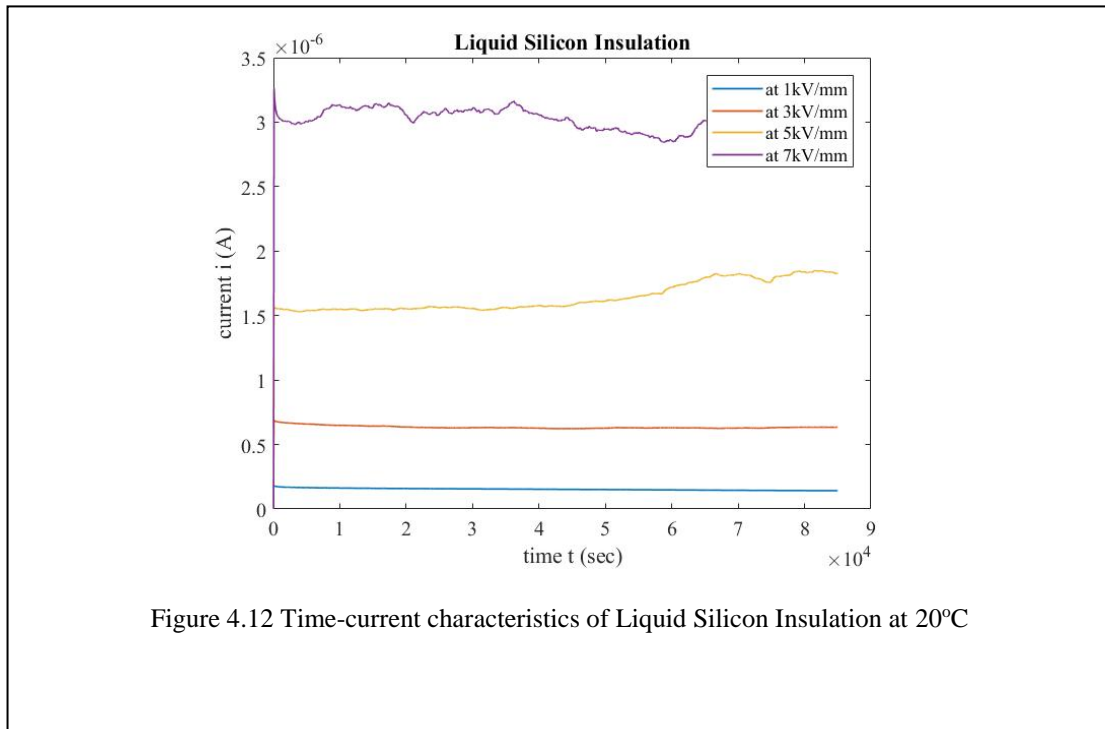


Figure 4.12 Time-current characteristics of Liquid Silicon Insulation at 20°C

To check if the variations could come from the fact that it was a new test cell, similar experiments were performed on Shell S4 mineral oil. The results are shown in figure 4.13. It is observed that there were no variations in shell S4 oil. This confirms that the variations in figure-4.12 at high electric field values are due to the liquid silicon insulation. Also, the conductivity of the shell S4 oil used was found to be 1.8×10^{-13} S/m at 1 kV/mm field and 24 hrs of energization time and 0.86×10^{-13} S/m at 5 kV/mm field and 24 hrs of energization time. This is similar to the conductivity values found in literature which confirms the correct working of the designed test cell.

The experiments were continued on a new sample of liquid silicon insulation, the time-current characteristics at 20°C and 40°C are shown in figure 4.14 and 4.15 respectively.

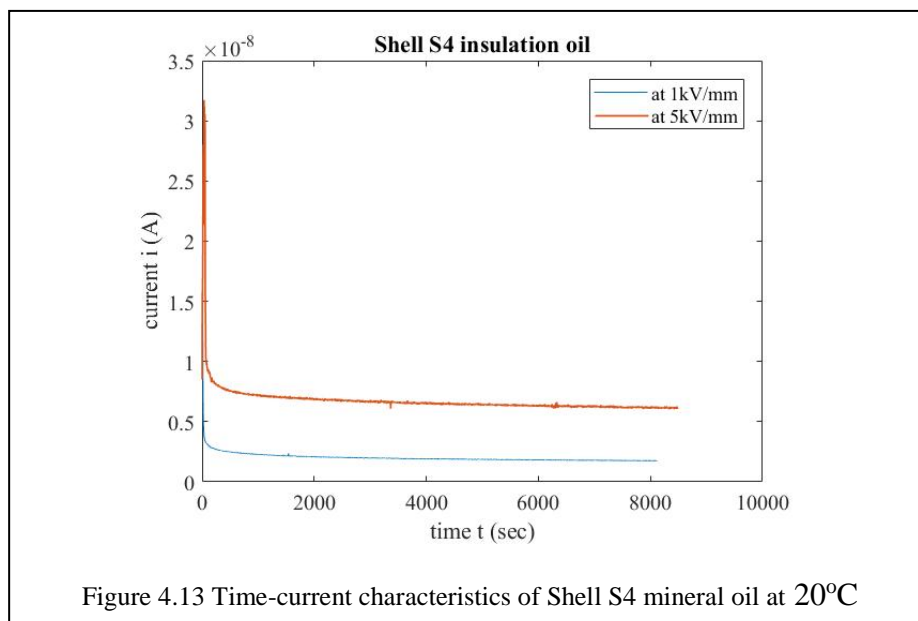
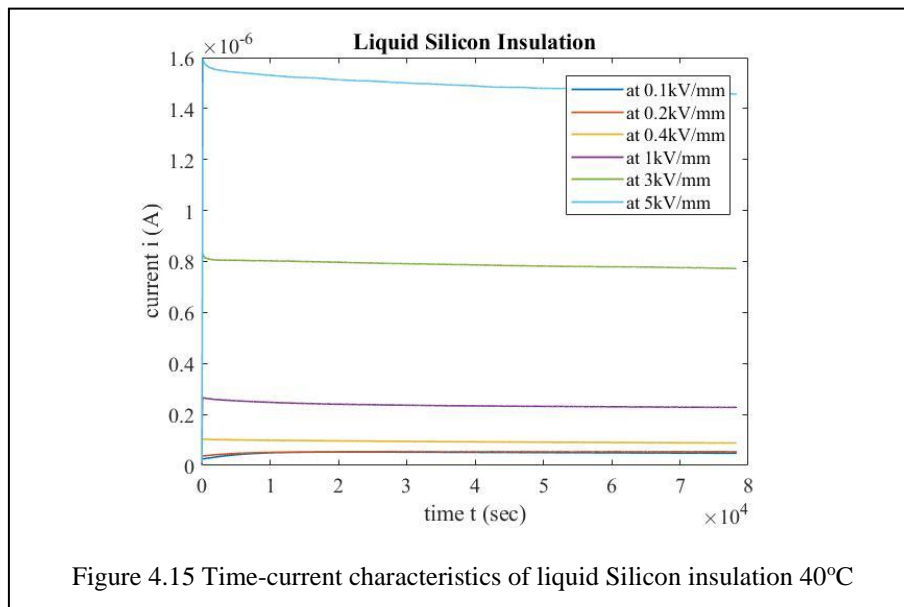
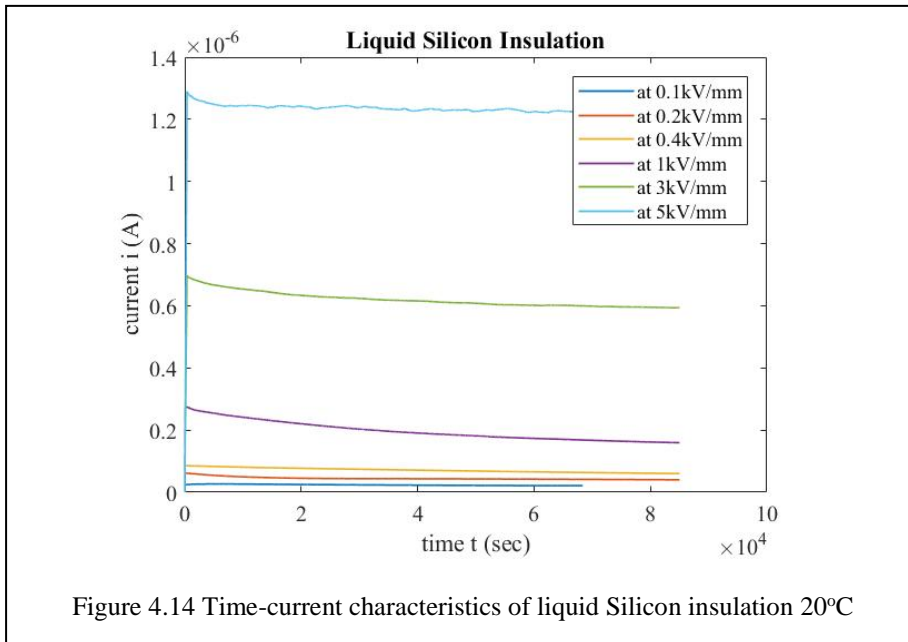
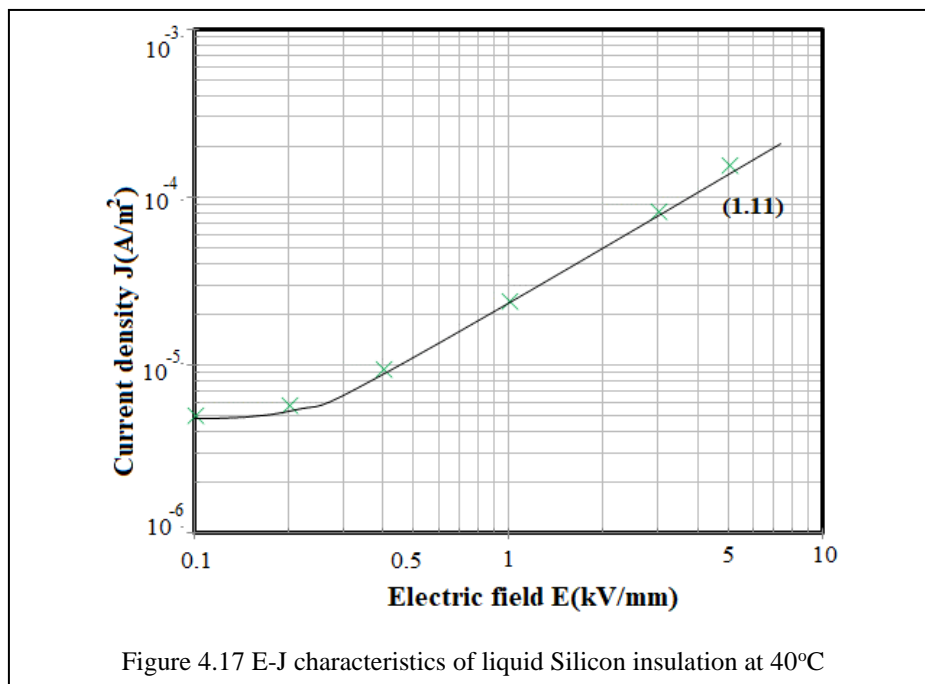
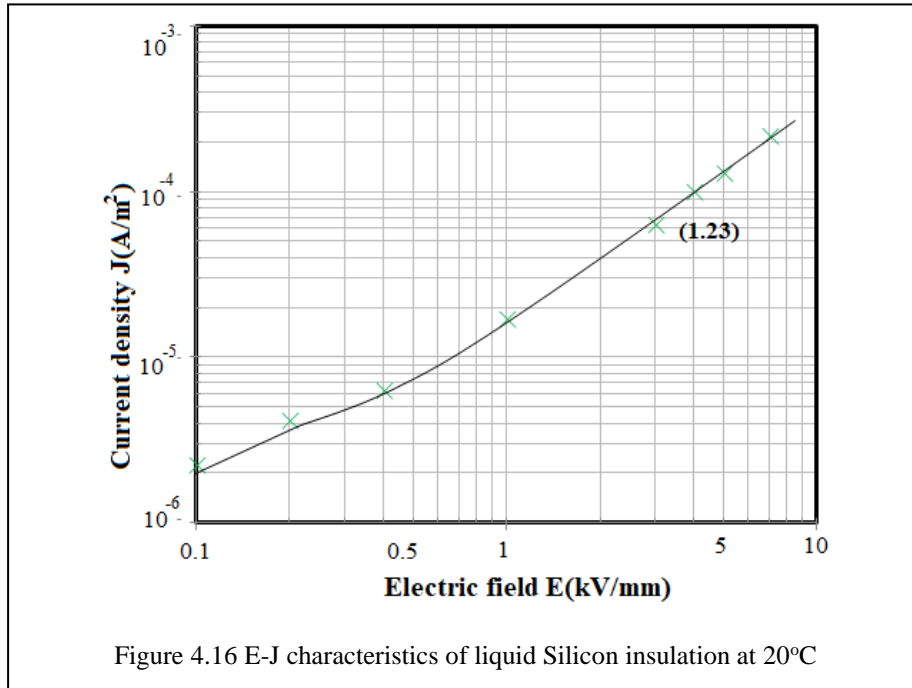


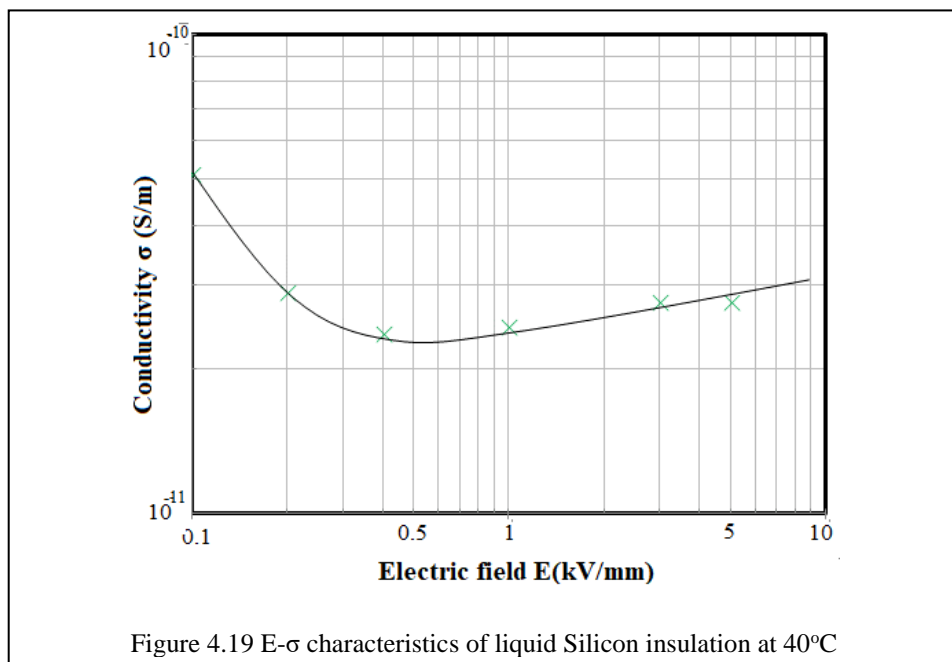
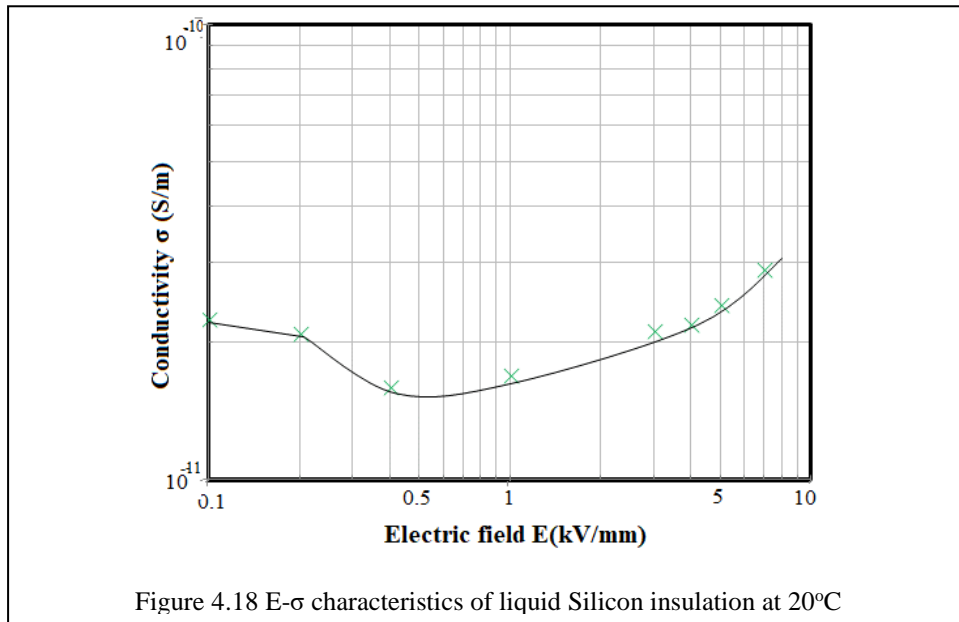
Figure 4.13 Time-current characteristics of Shell S4 mineral oil at 20°C



Figures-4.16 and 4.17 shows the plot of electric field (E) vs current density (J) and electric field (E) vs conductivity (σ) at 20°C respectively. Similar plots at 40°C are shown in figures-4.18 and 4.19 respectively.



From the electric field vs current density plots, it is seen that the slope of the line on log-log scale is nearly one, indicating an ohmic conduction.

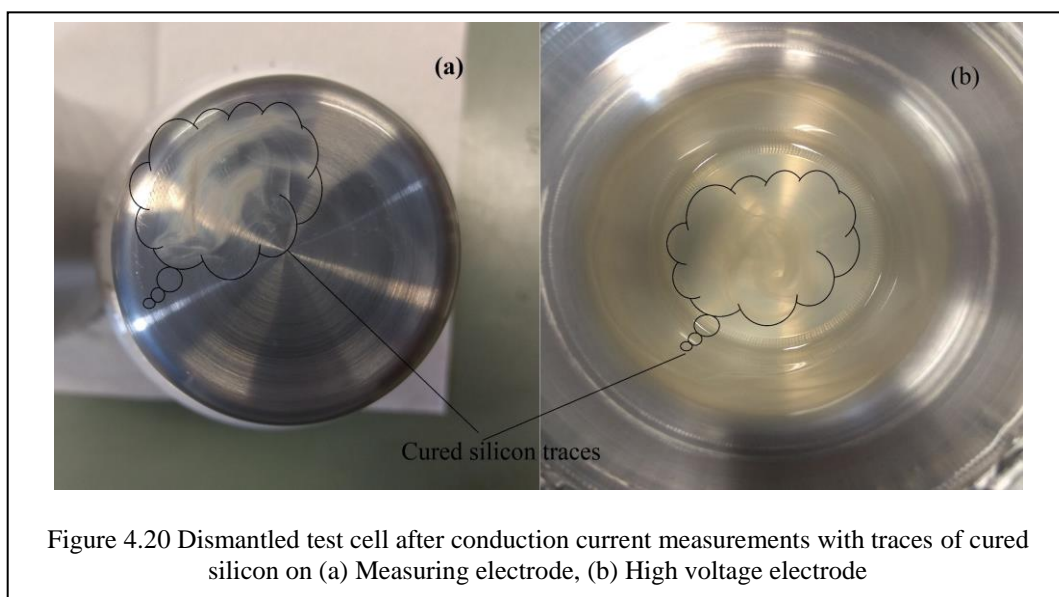


From the electric field vs conductivity plots it is observed that initially, conductivity is comparatively high and decreases with time of energization. It follows a “bath tub curve”. A similar behaviour was observed in [33]. This behaviour can be explained from ion generation and ion drift processes. Ions can be generated in two ways: in the bulk of the liquid or at the interfaces (metal-dielectric). At low electric field values, ions are transported under the electric field force to electrodes of opposite polarity. They are accumulated and/or partly neutralized by recombination processes. This field strength is not high enough to inject a significant number of electrons into the liquid. The ion drift velocity is higher at high electric field. So, at such high field strengths, more ions are accumulated in front of the counter electrodes and they form a new layer of charges with opposite magnitude as that of the

electrodes. These accumulated ions no longer contribute to the conduction current through the liquid. At field strength between 0.5-1 kV/mm, conductivity minimum is reached. Beyond this point, the increased electric field near the interfaces results in the generation of new charge carriers and thus conductivity increases.

The liquid silicon insulation is hygroscopic. It absorbs moisture to react and gets solidified. A sample of silicon insulation taken in a glass flask was degassed at a temperature of 60 °C to remove the moisture content. This temperature, instead of removing moisture content, supported the curing process and solidification was observed on the insulation surface. The Insulation bulk was still in liquid state.

A similar behaviour was observed in the conduction current measurement test cell. When the test cell was dismantled after a set of measurements, traces of solidification were observed. This is shown in figure-4.20.



4.1.3 Discussion on the results of conduction current measurements

From the conduction current measurements, effect of following parameters on the electrical conductivity can be described:

a. Time of energization:

From the time-current characteristics on liquid insulation (figures 4.12 to 4.15), it is seen that, there are no polarisation currents. And the initial high current value shifts steadily to a significantly lower steady state value. So, the time of energization for taking measurements plays an important role for the characterization of material under DC.

b. Influence of temperature:

In case of solid silicon insulation, with increasing temperature, the number of charge carriers and their mobility increases. This results in the increased electrical conductivity.

In liquid silicon insulation, according to Walden's rule, the product of viscosity (η) and ion mobility (μ) should remain constant at an equilibrium temperature. With increase in temperature, the viscosity of the insulation decreases, resulting in an increase in the ion mobility. This results in increase in the conductivity of the insulation.

The variations in the time-current characteristics are significant at 20°C and 5 kV/mm electric field. They are diminished with increasing temperature. This can be inferred to the increased mobility of the charge carriers and their recombination process at higher temperature. A similar behaviour is observed in [31].

c. Influence of Electric field strength:

The mobility of charge carriers increases with increasing electric field. This results in the increased electrical conductivity.

In solid silicon insulation, below the electric field threshold value, ohmic conduction is observed. The conductivity remains almost constant. Above the threshold value, in the super-ohmic region, conductivity increases with the electric field. The magnitude of the conductivity in this super-ohmic regime depends on the mechanisms involved in the conduction at the electric field.

In liquid insulation, the conductivity follows a 'bathtub curve' relation with the applied electric field. At a certain electric field value (0.4 kV/mm), maximum resistivity is obtained.

From table 4.1, it is observed that the conductivity of cured silicon is a strong function of electric field than temperature. Whereas for XLPE, the conductivity is a strong function of temperature than electric field. This property of cured silicon is more suitable for DC condition. Figure-4.21 shows the electric field distribution in a co-axial cylinder with XLPE and cured silicon insulation. It is seen that the electric field is more uniformly distributed with cured silicon insulation than with XLPE.

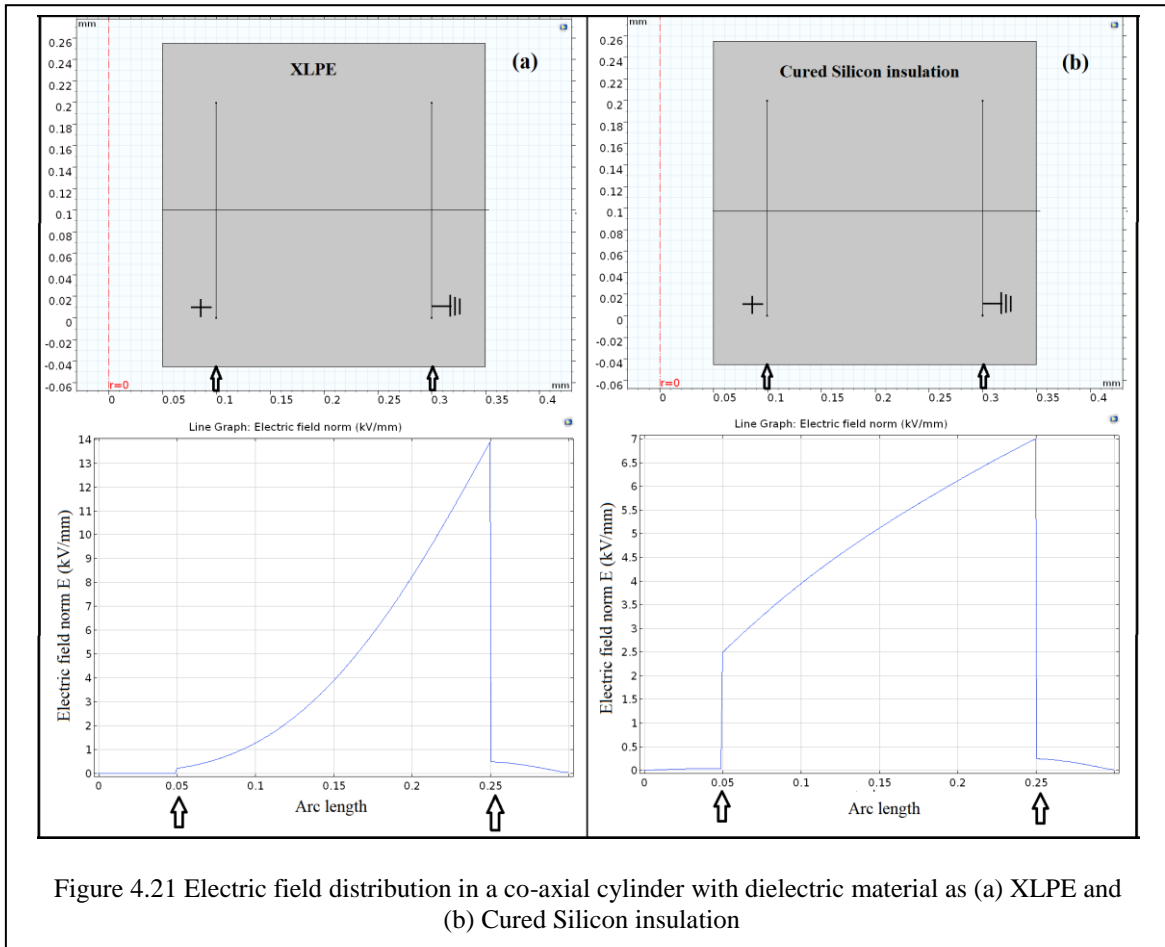


Figure 4.21 Electric field distribution in a co-axial cylinder with dielectric material as (a) XLPE and (b) Cured Silicon insulation

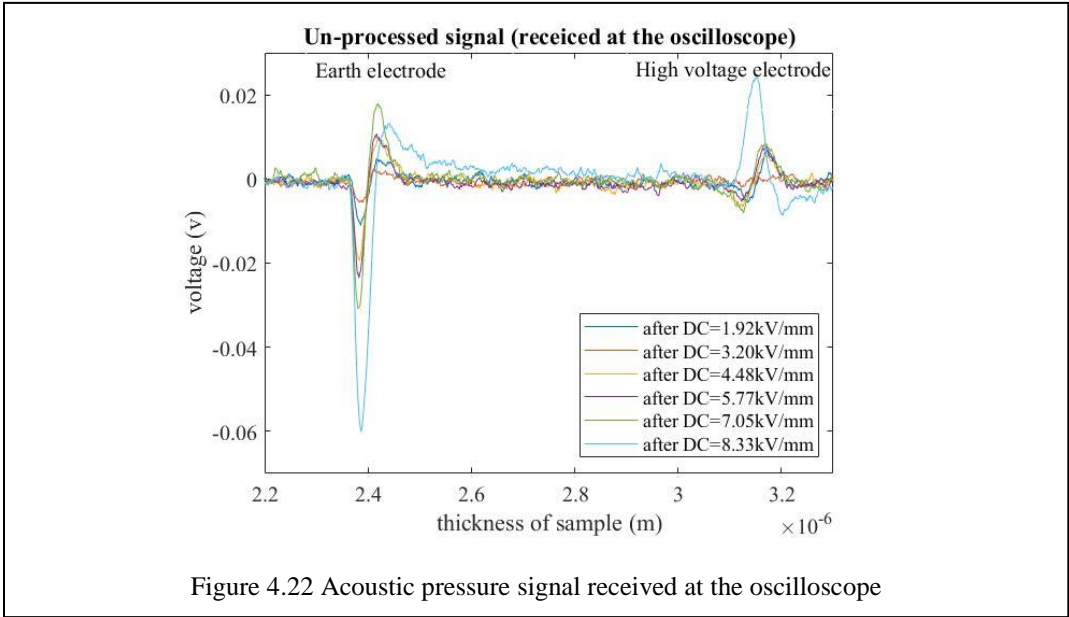
4.2 Space charge measurements using Pulsed Electro-acoustic method

The acoustic pressure wave signals received at oscilloscope for different values of the applied electric field are shown in figure-4.22. The post processing of these signals to get the space charge density value in the sample could not be performed. This is because of the following reasons:

- The insulation material is lossy (the signal at high voltage electrode got attenuated to $1/3^{\text{rd}}$ of its original value).
- Compression in the test sample was observed on the application of electric field. This is evident from the change in location of the peaks in figure-4.22.
- The gain of one of the amplifiers was not constant throughout the measurements as it was energized by a battery.
- Complete discharge of the samples was not possible due to the long-discharge time at ambient condition.

In figure-4.22, it can be observed that, peak values of the signal at both electrodes increases proportionally to the electric field in the range of 1.92 kV/mm till 7.05 kV/mm. At an electric field value of 8.33 kV/mm, a sudden increase in the peak values of the signals at both electrodes can be seen. This can be attributed to the onset of space charge accumulation in the

sample. In result, the electric field threshold value at ambient temperature is approximately 8.33 kV/mm. The electric field threshold value at ambient temperature calculated from conduction current measurements is 6 kV/mm. This difference in these values can be associated to the existence of semi conductive layer in the PEA method.



4.3 Cable Joint Simulations

Electric field plots along cut lines 1 – 4 for different scenarios in presence of temperature gradient of 30°C are shown in figures–4.21-4.24. The same plots when the temperature gradient is 60°C are shown in figures–4.25-4.28. The plot on top left in each figure represents the electric field distribution under AC condition. The top right plot represents the electric field distribution under DC condition when no cured silicon is present. The plot in the bottom of each figure represents the electric field distribution under DC when a cured silicon layer is present in the cable joint.

As expected, it is observed that, under AC conditions, presence of temperature gradient does not affect the Laplacian electric field distribution, since the electric field is dependent on the permittivity of materials. However, under DC condition, since the electric field is dependent on conductivity, electric field is inverted and significantly enhanced by the presence of temperature gradient. This electric field amplification is worsened by the presence of cured silicon layer in the cable joint.

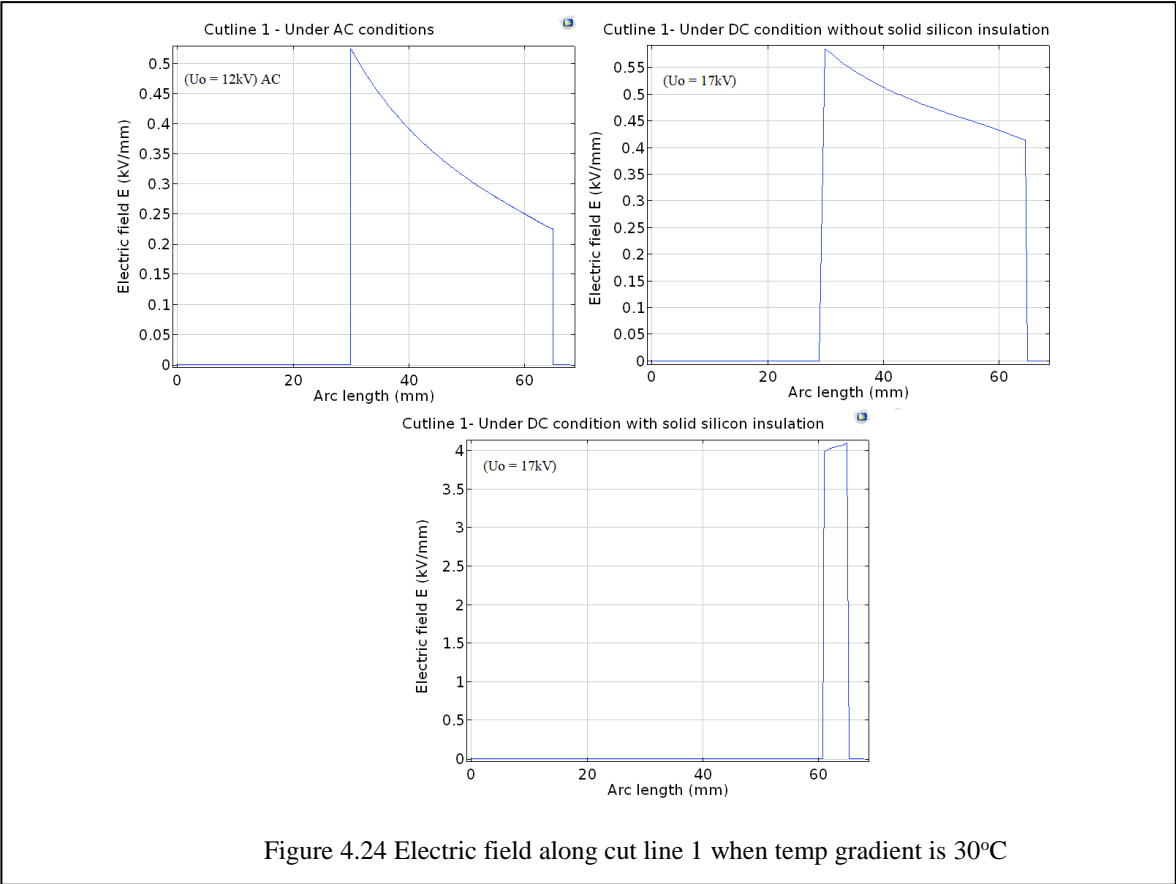


Figure 4.24 Electric field along cut line 1 when temp gradient is 30°C

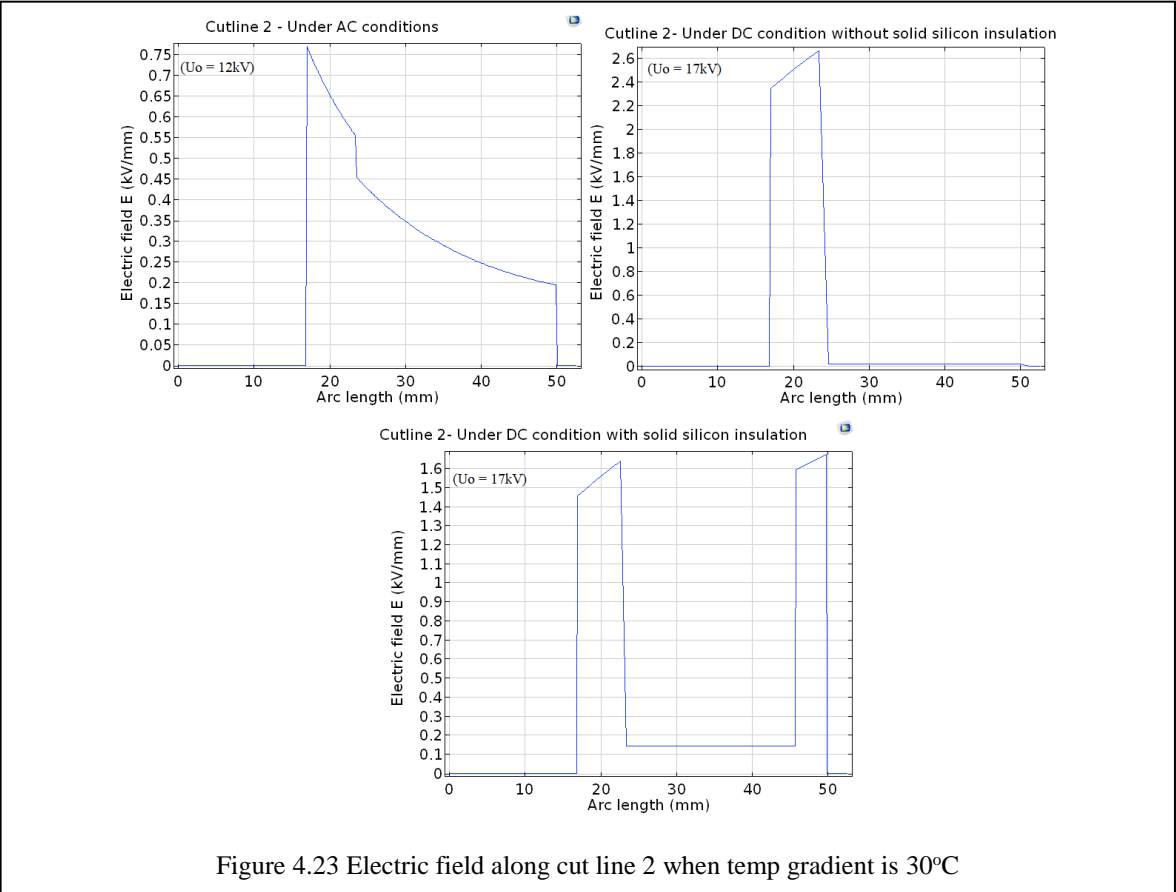


Figure 4.23 Electric field along cut line 2 when temp gradient is 30°C

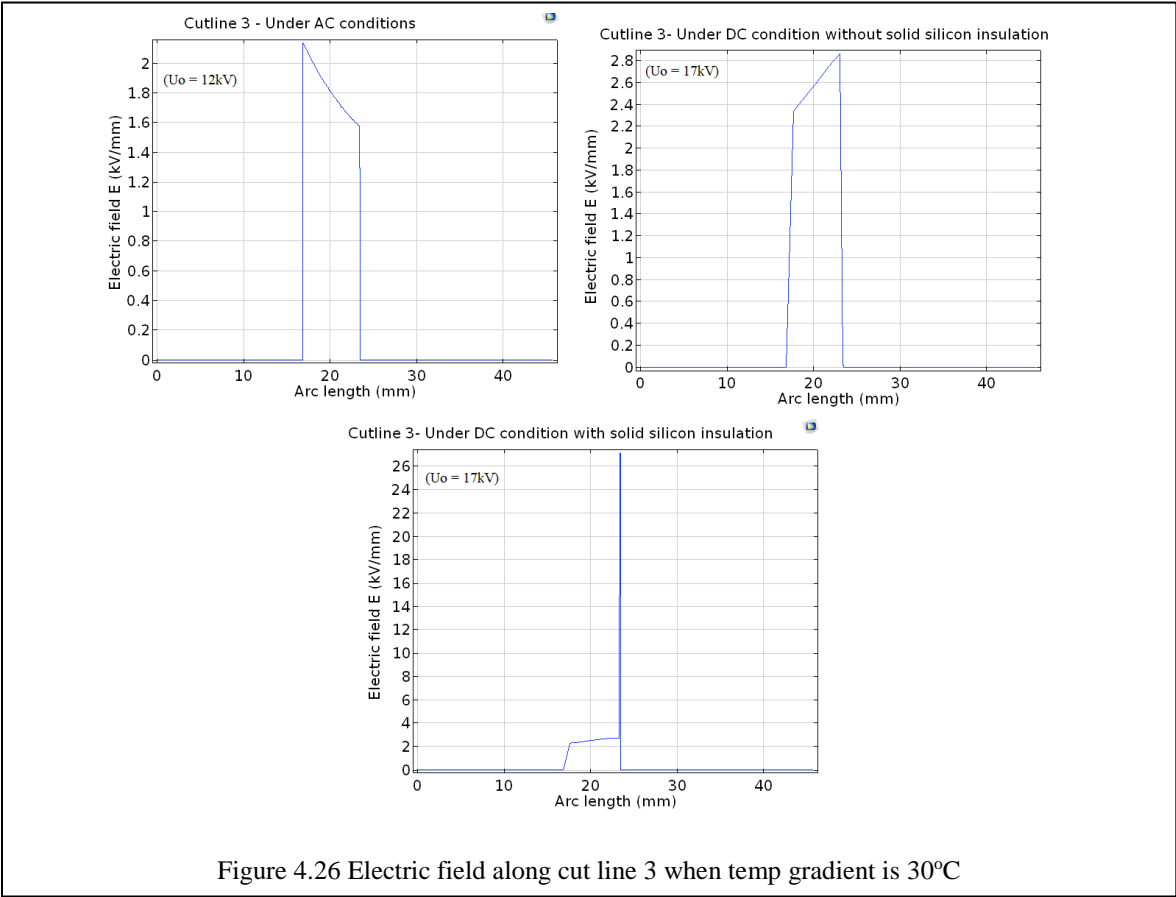


Figure 4.26 Electric field along cut line 3 when temp gradient is 30°C

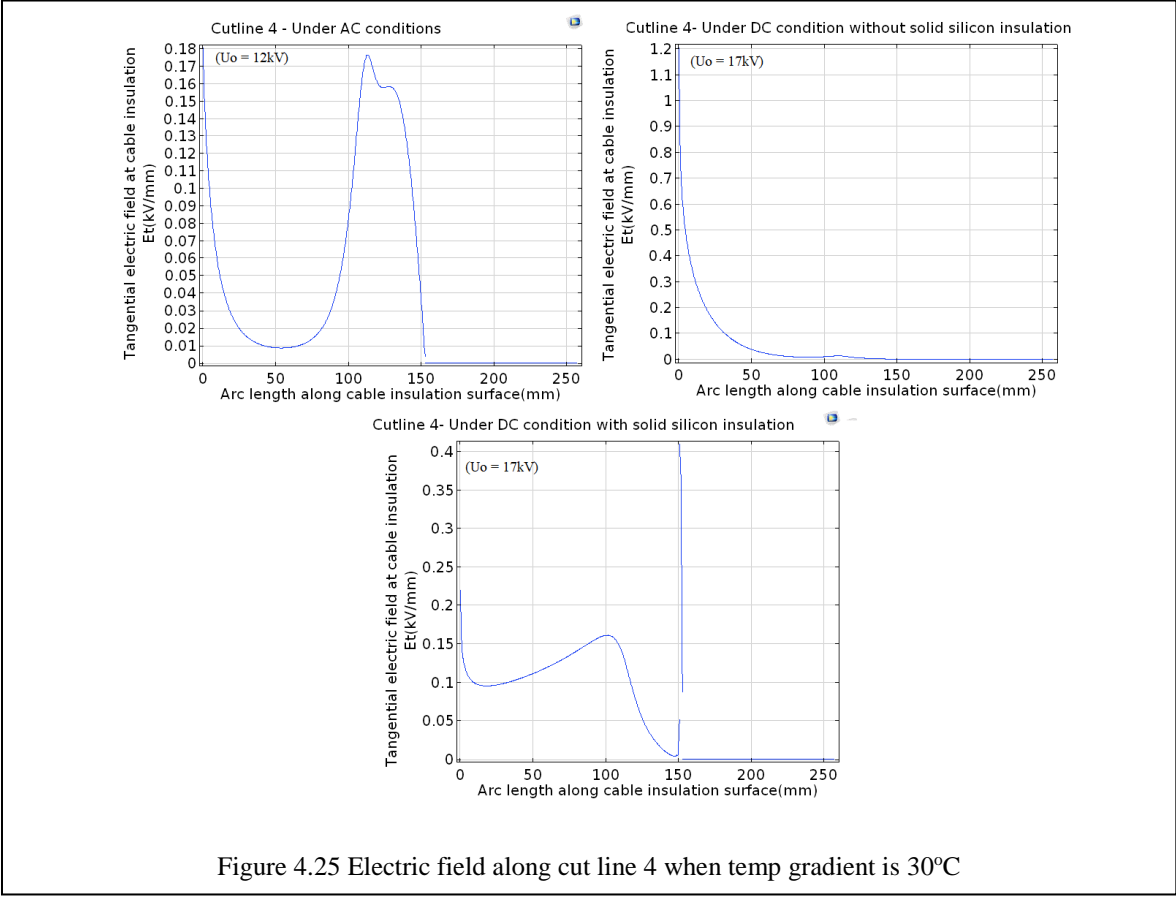


Figure 4.25 Electric field along cut line 4 when temp gradient is 30°C

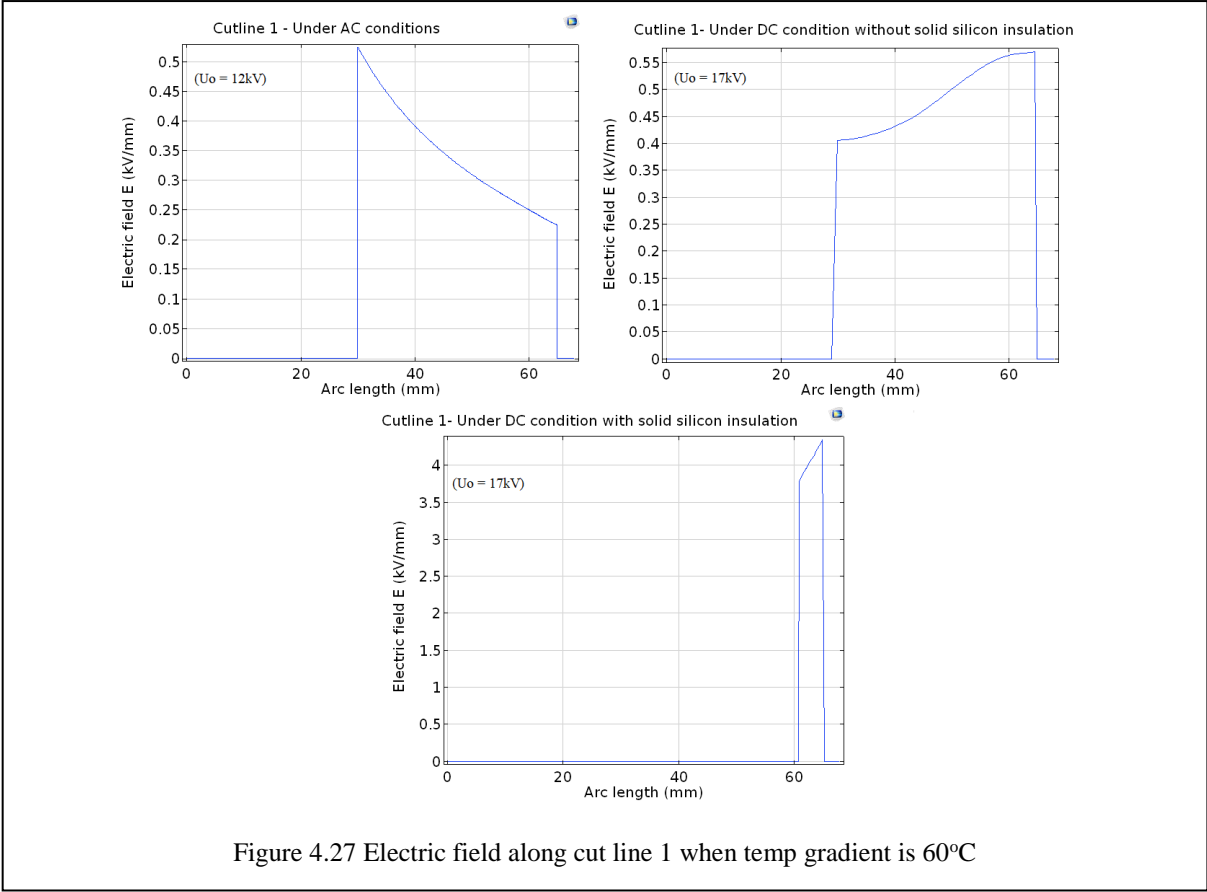


Figure 4.27 Electric field along cut line 1 when temp gradient is 60°C

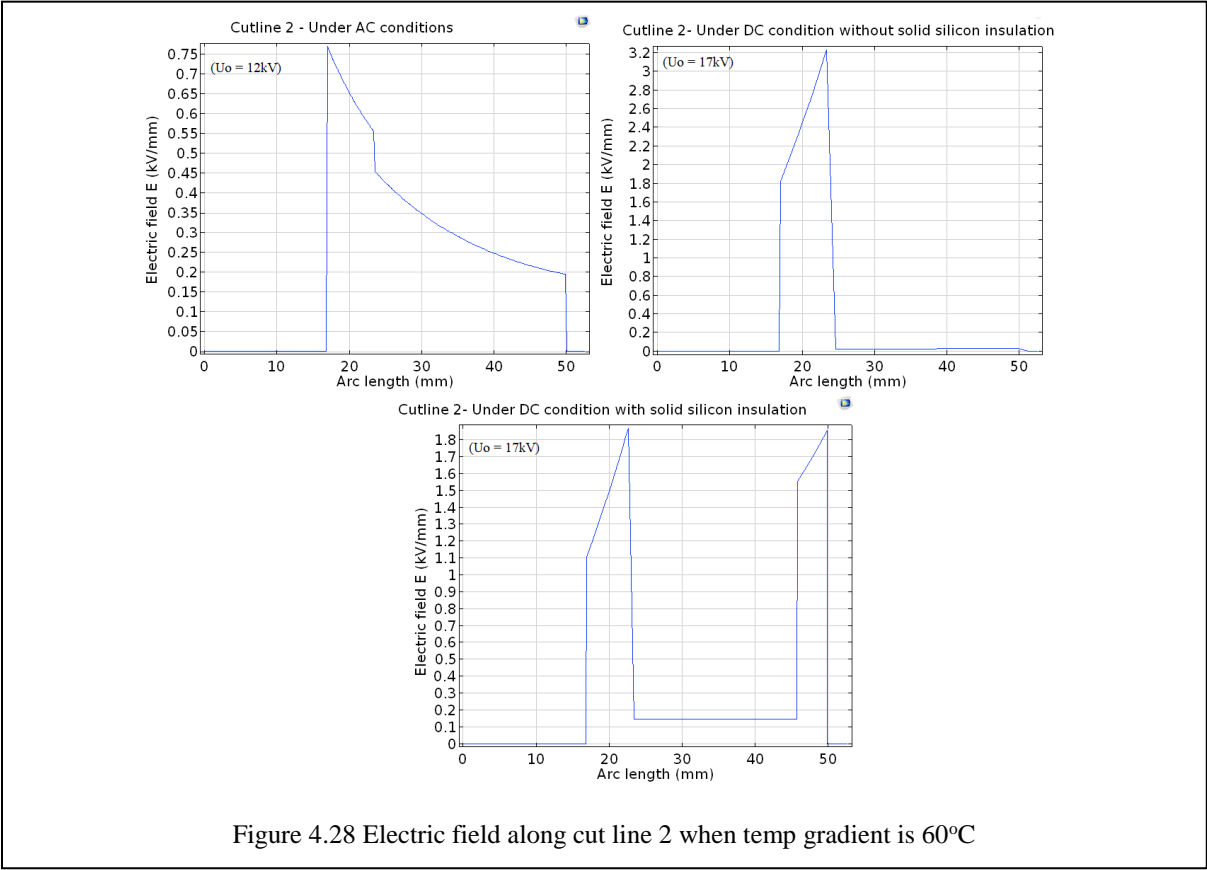


Figure 4.28 Electric field along cut line 2 when temp gradient is 60°C

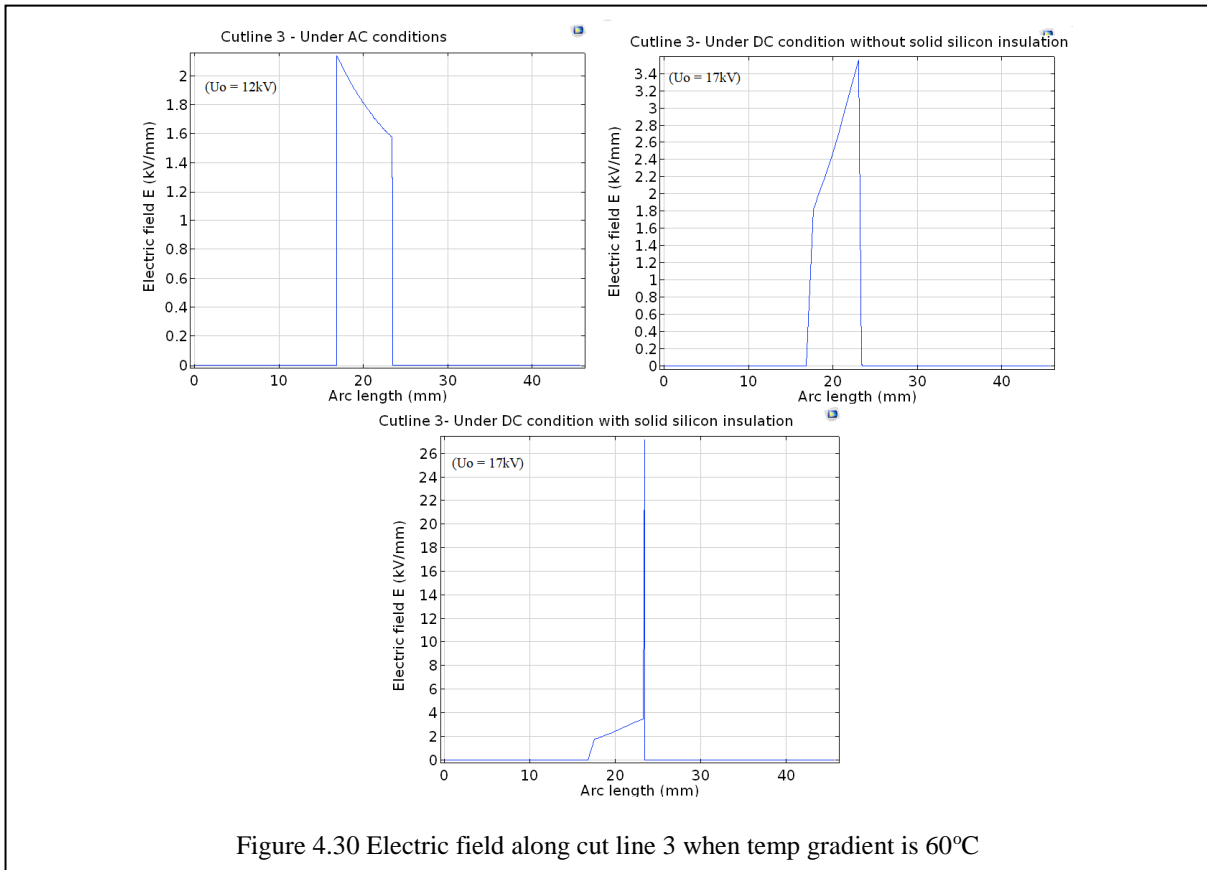


Figure 4.30 Electric field along cut line 3 when temp gradient is 60°C

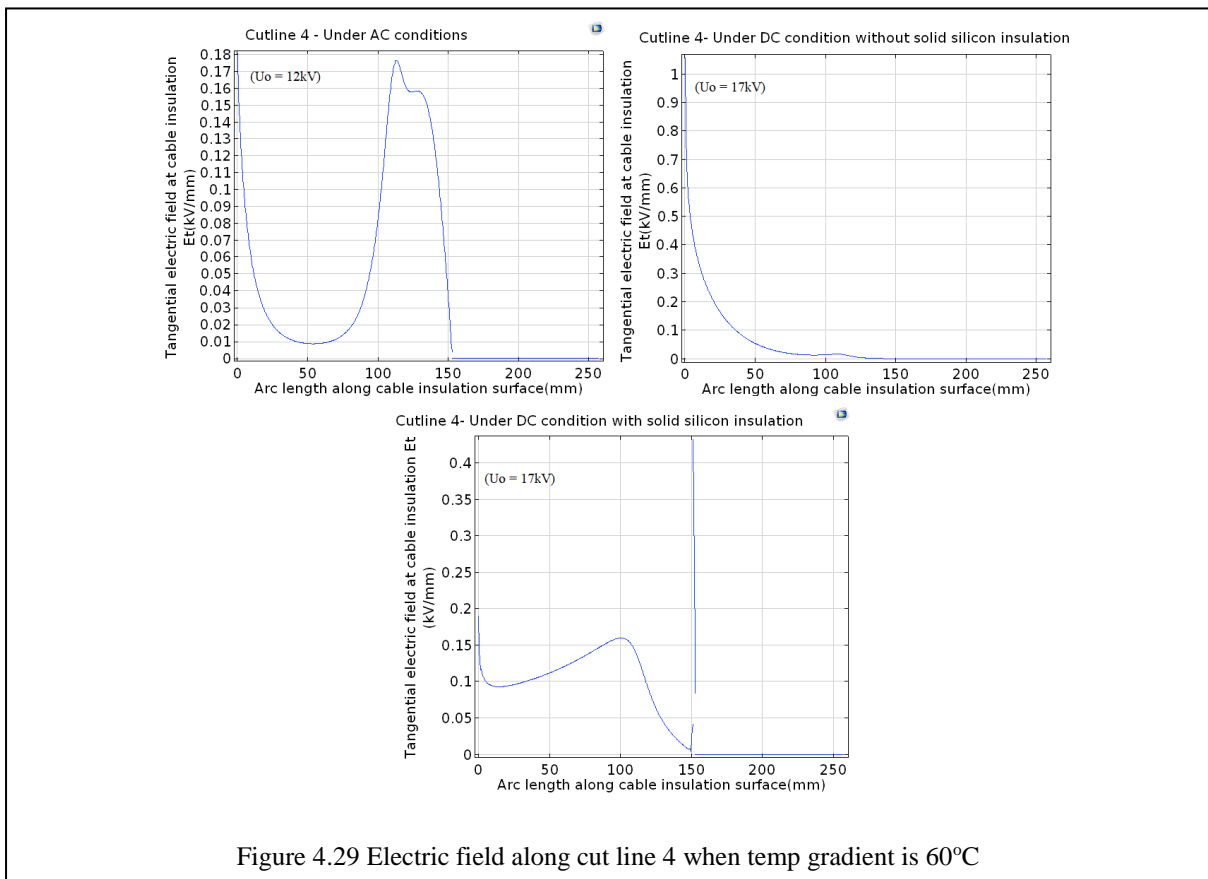


Figure 4.29 Electric field along cut line 4 when temp gradient is 60°C

As expected, the temperature dependent conductivities of the cable insulation (XLPE) and cable joint insulation (silicon insulation) resulted in the electric field inversion phenomenon.

The large difference in the conductivity values of the insulation materials resulted in high tangential electric field values under DC condition. Under AC condition, the value of tangential electric field is less because of small difference in the dielectric permittivity's of the insulation materials.

From the simulations it is observed that the presence of cured (solid) silicon layer inside cable joint under DC enhanced the electric field by 1200% the value at AC condition. The cured silicon layer is stressed by such a high value of electric field due to its lower conductivity.

The difference in conductivity values of XLPE, liquid silicon insulation and cured silicon insulation will result in the formation of surface charges as well as space charges, which is not investigated in this study.

5. Conclusions and Recommendations

The conclusions drawn from the conducted current measurements, space charge measurements and cable joint simulations are discussed in section 5.1. Section 5.2 contains some recommendations for further research into the characterization of material.

From the experimental results and the conclusions, the aim of this study to characterize silicon insulation material based on its conductivity behaviour under DC conditions and the electric field threshold for space charge formation is achieved fully.

5.1 Conclusions

A test cell has been developed capable of performing conduction current measurements with a breakdown strength of 25 kV DC. An electric field of maximum 12.5 kV/mm can be applied across the liquid insulation sample using this test cell.

The dielectric permittivity of cured silicon insulation is 2.6 and of the liquid silicon insulation is 2.9. Thus, under AC conditions, the presence of a cured silicon layer in the cable joint does not significantly enhance the electric field distribution. The permittivity being a weak function of temperature, remains almost constant. As a result, the electric field distribution in the cable joint does not change with the temperature.

The electrical conductivity of liquid silicon insulation at 0.4 kV/mm and 20°C is 1.6×10^{-11} S/m. Whereas the conductivity of cured silicon insulation at 2.5 kV/mm (ohmic region) and 20°C is 2.45×10^{-15} S/m. The presence of cured silicon layer in the cable joint under DC creates a divergent current density and significantly enhances the electric field distribution. This is evident from the electric field plots in section 4.2. It is seen that the electric field is concentrated in the cured silicon insulation layer.

The conductivity of the silicon insulation is a function of temperature and the electric field, this makes the electric field calculation in a cable joint complex under DC conditions. In result, it is difficult to design a proper insulation system.

From the values of electric field and temperature dependency coefficients of cured silicon sample in table 4.1, it can be concluded that the conductivity of cured silicon is a strong function of electric field than the temperature. Such a characteristic is more suitable for DC condition as it helps in distributing the inverted electric field uniformly. However, above electric field threshold value, the cured silicon insulation starts accumulating space charges. In the simulations performed on cable joint model, the difference in the conductivity values of liquid and cured silicon layer amplified the electric field in cured silicon layer by 120% than that under AC condition.

In case of liquid silicon sample, a 'bath tub curve' relation is observed for electric field vs conductivity.

5.2 Recommendations

In the present study, conduction current measurements are performed on silicon insulation material using aluminium electrodes considering the configuration in a real cable joint. From literature, it is found that the space charge effects in a dielectric depends on the electrode material. To study the behaviour of this insulation in other equipment's under DC condition, electrodes or semi conductive layers should be selected to simulate an actual configuration in the equipment.

The conduction current measurements provide an indication about the onset of space charges. Since the space charge phenomenon is space, time and temperature dependant, knowing the exact space charge distribution in sample could help in calculating the actual electric field distribution across the sample. Considering this, space charge measurements should be performed on the insulation samples in order to verify the electric field threshold values for space charge formation and to get the actual space charge distribution. These measurements also provide an information about the rate of space charge accumulated vs electric field. This information could be used to compare the insulating materials.

The conductivity of liquid silicon insulation follows a 'bath tub curve' with the electric field. This behaviour of the insulation material should be verified using the test cell mentioned in [31]. Since the electrical field distribution under DC is conductivity dependant, conductivity as a function of temperature and electric field should be used in the simulations.

References

- [1] Lovink Enertech, "Silicon insulation cable joints". Retrieved January 21, 2018, from <http://www.lovink-enertech.com/Cable-joints-LoviSil%C2%AE-.aspx?GB-12-3-0>
- [2] Reed, G.F., Grainger, B.M., Sparacino, A.R., Taylor, E.J., Korytowski, M.J., Mao, Z.H. "Medium Voltage DC Technology Developments, Applications, and Trends." In CIGRE US National Committee Grid of the Future Symposium, 2012.
- [3] Reed, Gregory F., Brandon M. Grainger, Adam R. Sparacino, and Zhi-Hong Mao. "Ship to grid: Medium-voltage DC concepts in theory and practice." *IEEE Power and Energy Magazine* 10, no. 6 (2012): 70-79.
- [4] Lundberg, Stefan. *Wind farm configuration and energy efficiency studies: series DC versus AC layouts*. Chalmers University of Technology, 2006.
- [5] Max, Lena, and Stefan Lundberg. "System efficiency of a DC/DC converter-based wind farm." *Wind Energy* 11, no. 1 (2008): 109-120.
- [6] Nguyen, Thai-Thanh, Hyeong-Jun Yoo, and Hak-Man Kim. "A comparison study of MVDC and MVAC for deployment of distributed wind generations." In *Sustainable Energy Technologies (ICSET), 2016 IEEE International Conference on*, pp. 138-141. IEEE, 2016.
- [7] G. McFadzean, C. Cleary, S. Hay, S. Dixon "The Potential Benefits of Direct-to-Shore MVDC Connections for Offshore Wind", *EWEA Offshore 2015*
- [8] Antoniou, Dimitris, Antonios Tzimas, and Simon M. Rowland. "Transition from alternating current to direct current low voltage distribution networks." *IET Generation, Transmission & Distribution* 9, no. 12 (2015): 1391-1401.
- [9] Shekhar, Aditya, Epameinondas Kontos, Armando Rodrigo Mor, Laura Ramírez-Elizondo, and Pavol Bauer. "Refurbishing existing mvac distribution cables to operate under dc conditions." In *Power Electronics and Motion Control Conference (PEMC), 2016 IEEE International*, pp. 450-455. IEEE, 2016.
- [10] Liu, Ying, Xiaolong Cao, and Mingli Fu. "The upgrading renovation of an existing XLPE cable circuit by conversion of AC line to DC operation." *IEEE Transactions on Power Delivery* 32, no. 3 (2017): 1321-1328.
- [11] Hampton, R. N. "Some of the considerations for materials operating under high-voltage, direct-current stresses." *IEEE Electrical Insulation Magazine* 24, no. 1 (2008): 5-13.
- [12] Kreuger, Frederik H. "Industrial high voltage: 1. fields, 2. dielectric, 3. constructions." (1991).

- [13] Zhang, Xiang, and Ernst Gockenbach. "Component reliability modeling of distribution systems based on the evaluation of failure statistics." *IEEE Transactions on Dielectrics and Electrical Insulation* 14, no. 5 (2007).
- [14] Khalil, M. Salah. "International research and development trends and problems of HVDC cables with polymeric insulation." *IEEE Electrical Insulation Magazine* 13, no. 6 (1997): 35-47.
- [15] Bodega, R., G. C. Montanari, and P. H. F. Morshuis. "Conduction current measurements on XLPE and EPR insulation." In *Electrical Insulation and Dielectric Phenomena, 2004. CEIDP'04. 2004 Annual Report Conference on*, pp. 101-105. IEEE, 2004.
- [16] Montanari, G. C. "The electrical degradation threshold of polyethylene investigated by space charge and conduction current measurements." *IEEE Transactions on Dielectrics and Electrical Insulation* 7, no. 3 (2000): 309-315.
- [17] Sanden, B., E. Ildstad, and R. Hegerberg. "Space charge accumulation and conduction current in XLPE insulation." In *Dielectric Materials, Measurements and Applications, Seventh International Conference on (Conf. Publ. No. 430)*, pp. 368-373. IET, 1996.
- [18] Alijagic-Jonuz, Belma. "Dielectric properties and space charge dynamics of polymeric high voltage DC insulating materials." PhD diss., TU Delft, Delft University of Technology, 2007.
- [19] Mazzanti, Giovanni, and Massimo Marzinotto. *Extruded cables for high-voltage direct-current transmission: advances in research and development*. Vol. 93. John Wiley & Sons, 2013.
- [20] Dissado, Len A., and John C. Fothergill. *Electrical degradation and breakdown in polymers*. Vol. 9. IET, 1992.
- [21] Moiz, Syed A., Iqbal A. Khan, Waheed A. Younis, and Khasan S. Karimov. "Space Charge-Limited Current Model for Polymers." In *Conducting Polymers*. InTech, 2016
- [22] Huber, P., and W. Kaiser. "Silicone fluids: synthesis, properties and applications." *Lubrication Science* 3, no. 2 (1986): 105-120.
- [23] Martin, Russell, Helen Athanassatou, Jean Claude Duart, Christophe Perrier, Ivan Sitar, Jeremie Walker, Clair Claiborne et al. "Experiences in service with new insulating liquids." *Working Group A2-35 CIGRE (2010)*: 1-95.
- [24] Liu, Peng, Zhen Xiang, Xin Ning, Hua Feng, and Zongren Peng. "Effect of electrode material on space charge behavior in epoxy resin." In *Electrical Insulation and Dielectric Phenomena (CEIDP), 2013 IEEE Conference on*, pp. 230-233. IEEE, 2013.
- [25] Tsekmes, Ioannis Alexandros. "Electrical Characterization of Polymeric DC Mini-Cables by means of Space Charge & Conduction Current Measurements." BEng Thesis, Delft University of Technology (2012).

- [26] Ahmed, N. H., and N. N. Srinivas. "Review of space charge measurements in dielectrics." *IEEE transactions on dielectrics and electrical insulation* 4, no. 5 (1997): 644-656.
- [27] Imburgia, Antonino, Rosario Miceli, Eleonora Riva Sanseverino, Pietro Romano, and Fabio Viola. "Review of space charge measurement systems: acoustic, thermal and optical methods." *IEEE Transactions on Dielectrics and Electrical Insulation* 23, no. 5 (2016): 3126-3142.
- [28] Takada, T., J. Holboell, A. Toureille, J. Densley, N. Hampton, J. Castellon, R. Hegerberg et al. "Guide for space charge measurements in dielectrics and insulating materials." *Electra* 223 (2005): 53-63.
- [29] Morshuis, Peter, and Marc Jeroense. "Space charge measurements on impregnated paper: a review of the PEA method and a discussion of results." *IEEE Electrical Insulation Magazine* 13, no. 3 (1997): 26-35.
- [30] Bodega, Riccardo. "Space charge accumulation in polymeric high voltage DC cable systems." (2006).
- [31] K uchler, Andreas, M. Liebschner, A. Reumann, Ch Krause, U. Piovan, B. Heinrich, R. Fritsche, J. Hoppe, A. Langens, and J. Titze. "Evaluation of conductivities and dielectric properties for highly stressed HVDC insulating materials." (2010).
- [32] Judendorfer, Thomas, Alexander Pirker, and Michael Muhr. "Conductivity measurements of electrical insulating oils." In *Dielectric Liquids (ICDL), 2011 IEEE International Conference on*, pp. 1-4. IEEE, 2011.
- [33] Schober, Fabian, Andreas K uchler, and Christoph Krause. "Oil conductivity–an important quantity for the design and the condition assessment of HVDC insulation systems." *Hochschule f ur angewandte Wissenschaften W urzburg-Schweinfurt (FHWS) Sci. J.* 1, no. 2 (2013): 59-78.

Acknowledgements

This thesis would never have been completed without the help of numerous people from TU Delft and Lovink Enertech that have supported the execution of this thesis.

Firstly, I would like to express my appreciation to Dr. A. Rodrigo Mor. His constant support and encouragement always motivated during the difficult phases of the thesis. Next I would like to thank Prof. Ir. Peter Vaessen for his invaluable contribution and support during this thesis work. Also, to Dr. Ir. Milos Cvetkovic for agreeing to be part of my thesis committee, devoting considerable time to the evaluation of this work in a timely manner.

I would also like to thank my company supervisors Ir. Aniket Lewarkar and Ir. Dennis Bergsma, for giving me the opportunity to work on and supporting me during my thesis project. Especially, I would like to thank Aniket for always taking his time when answering my questions. Besides my company supervisors, I would also like to thank Guillmero Mier Ecurra for his insightful feedback and guidance for the experiments performed.

Also, I wish to acknowledge the help provided by the staff of the high voltage lab. Ir. Paul Van Nes, Ir. Radek Heller, Ing. Remko Koornneef and Mr. Wim Termorshuizen were always available to help me. Their contribution to the construction of conduction current setup for liquids was significant.

Finally, I would like to thank my family and friends who always inspired, encouraged and supported me in every aspect of my life.

Satish Buddhawar
29th June 2018